

RECEIVED: December 3, 2021

REVISED: January 19, 2022

ACCEPTED: January 25, 2022

PUBLISHED: February 11, 2022

On-shell Z boson production at hadron colliders through $\mathcal{O}(\alpha\alpha_s)$

Roberto Bonciani,^a Federico Buccioni,^b Narayan Rana^{c,d} and Alessandro Vicini^d

^a*Dipartimento di Fisica, Università di Roma “La Sapienza” and INFN Sezione di Roma, Piazzale Aldo Moro 5, I-00185 Roma, Italy*

^b*Rudolf Peierls Centre for Theoretical Physics, Clarendon Laboratory, Parks Road, Oxford OX1 3PU, U.K.*

^c*Department of Physics, Indian Institute of Technology Kanpur, 208016 Kanpur, India*

^d*Dipartimento di Fisica “Aldo Pontremoli”, University of Milano and INFN Sezione di Milano, Via Celoria 16, 20133 Milano, Italy*

E-mail: roberto.bonciani@roma1.infn.it,

federico.buccioni@physics.ox.ac.uk, narayan.rana@unimi.it,

alessandro.vicini@mi.infn.it

ABSTRACT: The analytical expressions of the mixed QCD-EW corrections to on-shell Z boson inclusive production cross section at hadron colliders are presented, together with computational details. The results are given in terms of polylogarithmic functions and elliptic integrals. The impact on the prediction of the Z boson production total cross section is discussed, comparing different proton parton density sets.

KEYWORDS: Perturbative QCD, Scattering Amplitudes

ARXIV EPRINT: [2111.12694](https://arxiv.org/abs/2111.12694)

Contents

1	Introduction	1
2	The Z boson production cross section	3
2.1	The hadron-level cross section	3
2.2	The partonic subprocesses	5
2.2.1	Classification of the radiative corrections	8
2.2.2	Ultraviolet renormalisation	9
2.2.3	Infrared singularities and mass factorisation	10
3	Computational details	10
3.1	General strategy	10
3.2	Evaluation of the full set of master integrals	12
3.2.1	Example: a subsystem of two real-virtual master integrals	13
3.2.2	Solving the master integrals with elliptic kernels	15
4	Analytical results	18
4.1	Preliminaries: variables, functions and abbreviations	18
4.2	The virtual corrections	19
4.3	The partonic coefficients for QED	21
4.4	The partonic coefficients for Z	23
4.5	The partonic coefficients for W	27
4.6	Checks	36
5	Phenomenology	36
6	Conclusions	41

1 Introduction

The production in hadronic collisions of a pair of leptons, each with large transverse momentum, is known as Drell-Yan (DY) process and it plays a fundamental role for our understanding of Quantum Chromodynamics (QCD) as the theory of the strong interactions. The lepton pair acts as a probe of the initial-state proton structure. It allows for the measurement of the proton collinear parton density functions (PDFs) and for the study of the QCD dynamics from the analysis of the lepton-pair transverse momentum distribution. The kinematical distributions of the final-state leptons allow for precision tests of the electroweak (EW) Standard Model (SM), with the determination of the weak mixing angle [1, 2], and of the masses $m_{W,Z}$ [3, 4] of the W and Z bosons.

The production of an on-shell Z boson represents an approximation of the full neutral-current (NC) DY process, in that special kinematical configuration dominated by the Z -boson resonance. The total cross section of this process is an important theoretical benchmark constraining the proton PDFs, so that its prediction is a cornerstone in the precision physics program at hadron colliders. This process is described in lowest order (LO) by quark-antiquark annihilation into a Z boson via EW interaction. The evaluation of the next-to-leading order (NLO) [5], next-to-next-to-leading order (NNLO) [6–9], and next-to-next-to-next-to-leading order (N³LO) [10–14] QCD corrections to the production of an on-shell gauge boson, supplemented by the resummation of the logarithmically enhanced terms due to soft gluon emission [15–22], allows for the accurate estimate of the total cross section, the reduction of the impact of QCD uncertainty and the precise assessment of its actual size (cfr. also ref. [23]).

The best available QCD prediction for the inclusive production of a virtual gauge boson includes up to N³LO QCD corrections [12–14], in the γ^* , W , and in the complete NC DY cases respectively. It shows a dependence on the QCD renormalisation (μ_R) and factorisation (μ_F) scale choices at the sub-percent level for virtualities $Q > 70$ GeV and at the percent level for smaller Q values, with a stronger sensitivity to the choice of the factorisation scale.

In this high-precision QCD framework, the inclusion of EW effects becomes mandatory. The NLO-EW corrections to the DY process have been computed in [24–28] and are comparable in size to the NNLO-QCD effects. The theoretical uncertainty associated with missing higher-order EW corrections is formally at the NNLO-EW level and it is significantly reduced compared to the leading order (LO) case. Using different input parameters as a mean to estimate the size of missing higher-order EW effects, one finds that the LO variation is at the $\mathcal{O}(3.5\%)$ level, whereas the NLO-EW one is reduced down to the $\mathcal{O}(0.5\%)$ level. Despite of these significant progresses, it is possible to observe the presence of some residual sources of uncertainty in the results listed above. The higher-order QCD predictions are only LO accurate from the point of view of the EW interaction, and thus they suffer from the uncertainty associated with the different choices of input parameters. If we consider the NNLO-QCD prediction, supplemented with the NLO-EW one, we find a scheme uncertainty at the $\mathcal{O}(0.88\%)$ level. This value is significant for any precision test, it is comparable to the residual QCD uncertainty, and in any case is slightly larger than the corresponding estimate based only on the LO+ NLO-EW results. A specular discussion applies to the NLO-EW corrections, which are only LO from the point of view of the strong interaction. They suffer from large uncertainties under variations of the factorisation scale. The canonical μ_F variation by a factor 2 about its central value yields a change of the LO cross section by $\pm 18\%$ and, in turn, a change of the NLO-EW correction at the $\mathcal{O}(0.5\%)$ level. In order to increase the control on the theoretical error, it is therefore mandatory to include in the analysis the full mixed QCD-EW corrections, since they stabilize both the dependence on the QCD scales of the higher-order EW corrections and the dependence on the EW input parameters of the higher-order QCD corrections.

The mixed corrections to the DY process in the resonance region have been studied in the so-called pole approximation in refs. [29, 30], where QCD and EW effects are factorised

between production and decay of the vector boson. As far as the production of an on-shell Z boson is concerned, the exact QCD-QED corrections have been considered in refs. [31–33], while in [34–36] we have computed the mixed QCD-EW effects fully analytically for the inclusive production. In ref. [37], the fully differential QCD×EW effects have been presented, using a combination of analytical and numerical techniques. As for the full neutral-current DY, the QCD×QED corrections to the production of a pair of neutrinos have been discussed in ref. [38], and the complete NNLO QCD-EW corrections for a charged lepton pair in the final state have been presented in [39, 40]. Considering pole-approximation only for the virtual contributions, the QCD-EW corrections to the charged current DY has been obtained in [41].

In this paper, we explicitly present the analytical expressions and all the computational details to obtain the $\mathcal{O}(\alpha\alpha_s)$ mixed QCD-EW corrections to on-shell Z boson inclusive production cross section at hadron colliders. The results have been fully computed in analytical form and expressed in terms of polylogarithmic functions and elliptic integrals, requiring the evaluation of new two-loop master integrals (MIs) that were not available in the literature. The inclusion of the $\mathcal{O}(\alpha\alpha_s)$ corrections increases the accuracy of the prediction and it reduces the impact of the residual theoretical uncertainties. The evaluation of the hadron-level cross section requires the convolution of the partonic results with proton PDFs. For consistency, the latter must satisfy DGLAP equations with also a QCD+QED evolution kernel. We comment on the accuracy of our predictions, compared to a standard analysis that includes only QCD corrections.

2 The Z boson production cross section

In this section, we discuss the theoretical framework, providing the details of perturbative contributions from various partonic channels which constitute the mixed QCD-EW corrections to the inclusive production cross section of the Z boson at hadron colliders. We also discuss here the necessary steps to perform ultraviolet (UV) renormalisation and mass factorisation.

2.1 The hadron-level cross section

We organize the hadron-level inclusive Z production cross section as a double perturbative expansion in the QCD and EW couplings, α_s and α , respectively:

$$\sigma_H \equiv \sigma(h_1 h_2 \rightarrow Z + X) = \sum_{m=0}^{\infty} \sum_{n=0}^{\infty} \alpha_s^m \alpha^n \sigma^{(m,n)}. \quad (2.1)$$

The first term of this expansion, $\sigma^{(0,0)}$ is called Born cross section. All the contributions of $\mathcal{O}(\alpha_s)$ with respect to the Born form the NLO-QCD corrections $\sigma^{(1,0)}$, those of $\mathcal{O}(\alpha)$ are the NLO-EW corrections $\sigma^{(0,1)}$. At the second orders, the $\mathcal{O}(\alpha_s^2)$, $\mathcal{O}(\alpha^2)$ and $\mathcal{O}(\alpha\alpha_s)$ contributions are called the NNLO-QCD ($\sigma^{(2,0)}$), NNLO QCD-EW ($\sigma^{(1,1)}$) and NNLO EW ($\sigma^{(0,2)}$) corrections, respectively. In this paper we describe in detail the complete computation of $\sigma^{(1,1)}$.

The hadron-level cross section for the inclusive production of an on-shell Z boson can be written, according to the factorisation theorem, as

$$\sigma_H = \sum_{i,j=q,\bar{q},g,\gamma} \int_0^1 dx_1 \int_0^1 dx_2 \tilde{f}_i^{h_1}(x_1) \tilde{f}_j^{h_2}(x_2) \tilde{\sigma}_{ij}. \quad (2.2)$$

The bare PDFs, $\tilde{f}_i^h(x)$, describe the partonic content of the hadron h , where i can be a quark (q), anti-quark (\bar{q}), gluon (g) or photon (γ). The partonic cross section $\tilde{\sigma}_{ij} \equiv \tilde{\sigma}(ij \rightarrow Z + X)$, describes the inclusive production of a Z boson in the scattering of partons i and j .

In the evaluation of the radiative corrections, the presence of UV and IR divergences is handled in dimensional regularisation, with $d = 4 - 2\epsilon$ being the number of space-time dimensions. The individual matrix elements contain in general poles in ϵ . The cancellation of the UV singularities takes place via UV renormalisation. The combination of virtual and soft real emission corrections to the same underlying process leads to a cancellation of the IR soft poles. According to the Kinoshita-Lee-Nauenberg (KLN) theorem [42, 43], the combination of the different partonic cross sections contains only singularities due to the emission of collinear partons from the initial state. The latter are universal, they can be factorised and reabsorbed in the definition of the physical proton PDFs, $f_i(x, \mu_F) = \Gamma_{ik}(\mu_F) \tilde{f}_k(x)$, by means of the mass factorisation kernel Γ , defined at the factorisation scale μ_F . As a consequence, eq. (2.2) can be written as follows with the convolution represented by the symbol \otimes ,

$$\begin{aligned} \sigma_H &= \sum_{i,j=q,\bar{q},g,\gamma} \int_0^1 dx_1 \int_0^1 dx_2 f_i^{h_1}(x_1, \mu_F) f_j^{h_2}(x_2, \mu_F) \Gamma_{ik}^{-1}(\mu_F) \Gamma_{jl}^{-1}(\mu_F) \tilde{\sigma}_{kl}(x_1, x_2), \\ &\equiv \sigma_0 \sum_{i,j=q,\bar{q},g,\gamma} f_i^{h_1}(\mu_F) \otimes f_j^{h_2}(\mu_F) \otimes \Delta_{ij}(\mu_F). \end{aligned} \quad (2.3)$$

The constant σ_0 is defined through the Born cross section $\sigma^{(0,0)}$,

$$\sigma^{(0,0)} \equiv \sigma_0 c_q^{(0)} \delta(1-z) = \frac{4\sqrt{2}\pi}{N_C} G_\mu c_q^{(0)} \delta(1-z). \quad (2.4)$$

In the latter, $z \equiv m_Z^2/\hat{s}$, $\sqrt{\hat{s}}$ is the partonic center of mass energy, N_C is the number of colors, and $c_q^{(0)} = (C_{v,q}^2 + C_{a,q}^2)$ is the combination of charges of the coupling of the Z boson to a quark q . $C_{v,q}$ and $C_{a,q}$ are given by

$$C_{v,q} = \left(\frac{I_W^{(q)}}{2} - \sin \theta_W Q_q \right), \quad C_{a,q} = \left(\frac{I_W^{(q)}}{2} \right), \quad (2.5)$$

with $I_W^{(q)}$ and Q_q the third component of the weak isospin and the electric charge in units of the positron charge, respectively. θ_W is the weak mixing angle.

Δ_{ij} is the UV- and IR-finite partonic cross section for the partonic channel ij , expressed in units σ_0 . In perturbation theory, Δ_{ij} is expanded in series of α_s and α as

$$\Delta_{ij} = \sum_{m=0}^{\infty} \sum_{n=0}^{\infty} \alpha_s^m \alpha^n \Delta_{ij}^{(m,n)}. \quad (2.6)$$

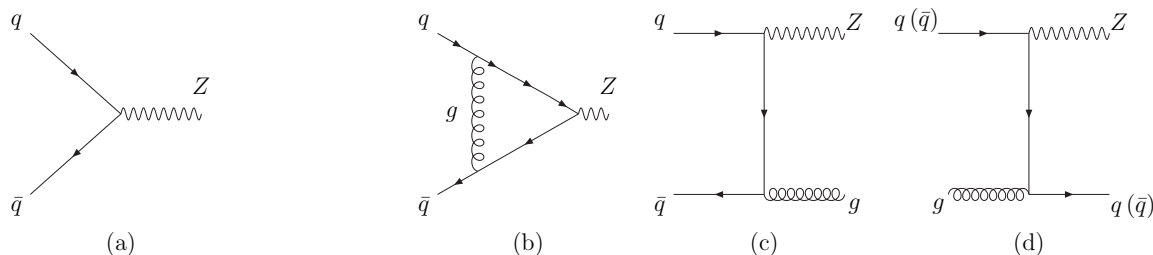


Figure 1. Feynman Diagrams contributing to the Born (a) and to the $\mathcal{O}(\alpha_s)$ corrections (b)–(d) to the production of a Z boson in hadronic collisions. Crossed diagrams are not shown.

The main results of this paper are the expressions of the corrections $\Delta_{ij}^{(1,1)}$ with $i, j = q, \bar{q}, g, \gamma$. In the study of the NNLO QCD-EW corrections, we encounter different gauge invariant subsets, characterised by the exchange of additional photons or massive weak bosons W s or Z s. We reorganize accordingly the total $\mathcal{O}(\alpha_s)$ correction, introducing

$$\alpha\alpha_s\sigma^{(1,1)} = \sigma_0 \frac{\alpha}{4\pi} \frac{\alpha_s}{4\pi} \left(\Delta_\gamma^{(1,1)} + \frac{1}{s_W^2 c_W^2} \Delta_Z^{(1,1)} + \frac{1}{s_W^2} \Delta_W^{(1,1)} \right). \quad (2.7)$$

We present in section 4 the expressions of $\Delta_\gamma^{(1,1)}$, $\Delta_Z^{(1,1)}$, and $\Delta_W^{(1,1)}$.

2.2 The partonic subprocesses

The inclusive production cross section receives, order by order in perturbation theory, virtual as well as real emission corrections. The additional final-state partons present in the latter are completely integrated over their respective phase space. The first term of the expansion $\sigma^{(0,0)}$ in eq. (2.1), receives contributions from the single partonic process (see figure 1 (a))

$$q + \bar{q} \rightarrow Z. \quad (2.8)$$

$\sigma^{(1,0)}$ in eq. (2.1) receives contributions from the partonic processes

$$q + \bar{q} \rightarrow Z, \quad q + \bar{q} \rightarrow Z + g, \quad q + g \rightarrow Z + q. \quad (2.9)$$

The first process receives NLO-QCD virtual corrections (figure 1 (b)), while the other two are evaluated at tree level, with the phase-space of the emitted parton (g/q) integrated out (figure 1 (c),(d)). In case of $\sigma^{(0,1)}$, the processes are (see figure 2)

$$q + \bar{q} \rightarrow Z, \quad q + \bar{q} \rightarrow Z + \gamma, \quad q + \gamma \rightarrow Z + q, \quad (2.10)$$

where the first process receives NLO-EW virtual corrections (figure 2 (a)). At $\mathcal{O}(\alpha\alpha_s)$ we have double-virtual, real-virtual and double-real contributions. Double-virtual corrections are two-loop contributions, with one gluon and one/two EW gauge bosons in the loop, to the partonic process (see figure 3)

$$q + \bar{q} \rightarrow Z. \quad (2.11)$$

In the real-virtual contributions we find one virtual loop and one real-emitted particle. The

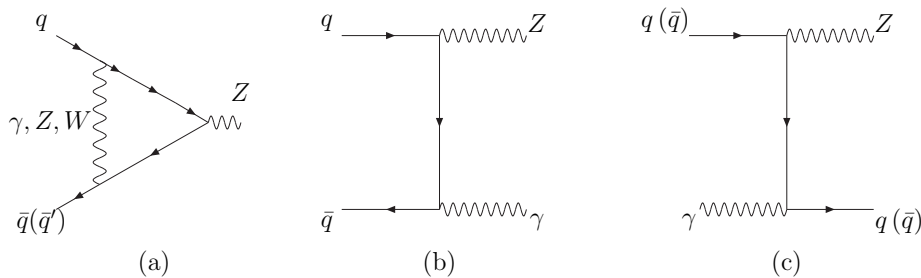


Figure 2. Feynman Diagrams contributing to the $\mathcal{O}(\alpha)$ corrections to the production of a Z boson in hadronic collisions. Crossed diagrams are not shown.

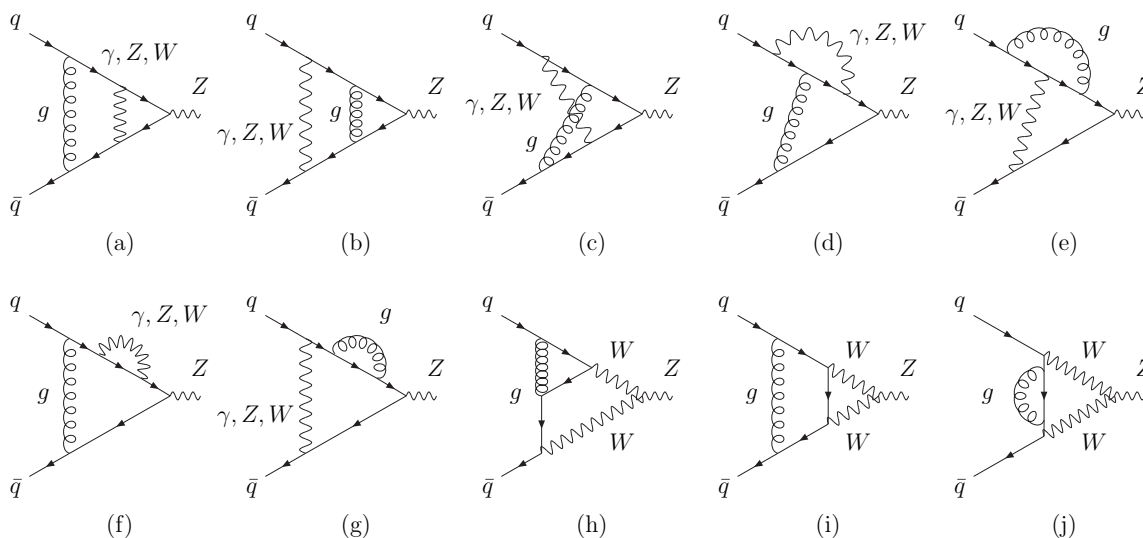


Figure 3. Two-loop Feynman Diagrams contributing to the $\mathcal{O}(\alpha\alpha_s)$ corrections to the production of a Z boson in hadronic collisions, eq. (2.11). Symmetric diagrams are not shown.

processes which contribute to this group are (see figure 4)

$$q + \bar{q} \rightarrow Z + g, \quad q + g \rightarrow Z + q, \quad q + \bar{q} \rightarrow Z + \gamma, \quad q + \gamma \rightarrow Z + q. \quad (2.12)$$

For the first two processes, the loop integral is of $\mathcal{O}(\alpha)$ (figure 4(a)–(h)), while for the others it is of $\mathcal{O}(\alpha_s)$ (figure 4(i)–(p)). At $\mathcal{O}(\alpha\alpha_s)$, the double-real contributions are with two real-emitted partons. Their amplitudes are evaluated at tree level. In the cases with two (anti)quarks in the initial and two (anti)quarks in the final state, in addition to the Z , the scattering is mediated by either a gluon or an EW boson, so that the respective contributions have a different proportionality in terms of α and α_s . The interference between the two groups of contributions is of $\mathcal{O}(\alpha\alpha_s)$ with respect to the Born process and is relevant for the calculation of $\sigma^{(1,1)}$. The complete list of processes is (see figure 5)

$$\begin{aligned} q + \bar{q} &\rightarrow Z + g + \gamma, & q + \bar{q} &\rightarrow Z + q + \bar{q}, & q + q &\rightarrow Z + q + q, \\ q + g &\rightarrow Z + q + \gamma, & q + \gamma &\rightarrow Z + g + q, & g + \gamma &\rightarrow Z + q + \bar{q}, \\ q + q' &\rightarrow Z + q + q', & q + \bar{q} &\rightarrow Z + q' + \bar{q}', & q + \bar{q}' &\rightarrow Z + q + \bar{q}'. \end{aligned} \quad (2.13)$$

We denote with q' a different quark flavour.

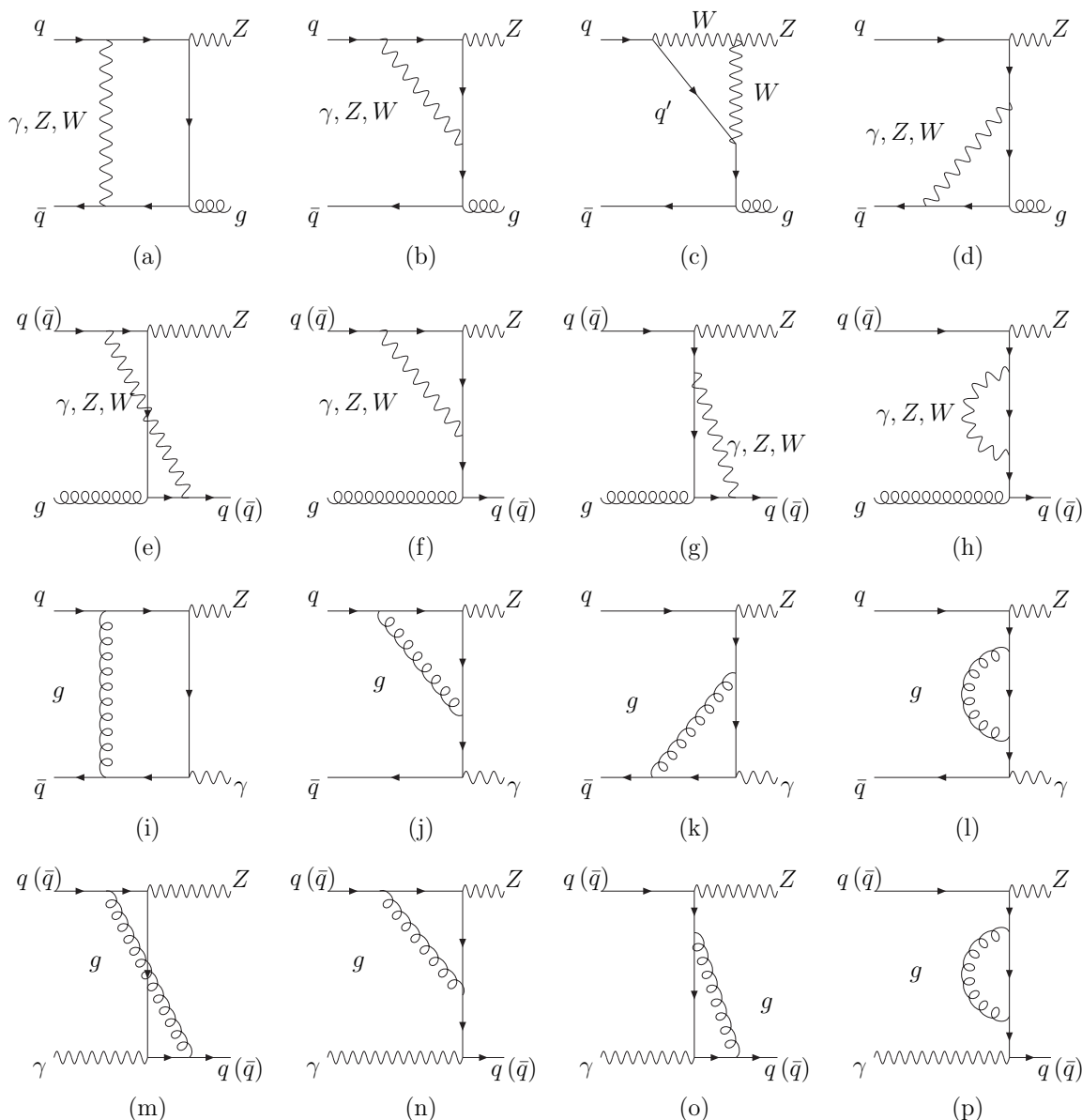


Figure 4. Examples of Feynman Diagrams contributing to the real-virtual corrections to the production of a Z boson in hadronic collisions, eqs. (2.12).

We analytically compute the contribution at $\mathcal{O}(\alpha\alpha_s)$ to the total cross section of each of the above listed processes, which can be presented as a Laurent expansion in ε . After the combination of all the degenerate states and mass factorisation, the singularities cancel and the remaining non-vanishing finite contributions are the factors $\Delta_{ij}^{(1,1)}$. We present in section 4 their analytical expressions, and provide them also in a **Mathematica** supplementary file attached to this paper.

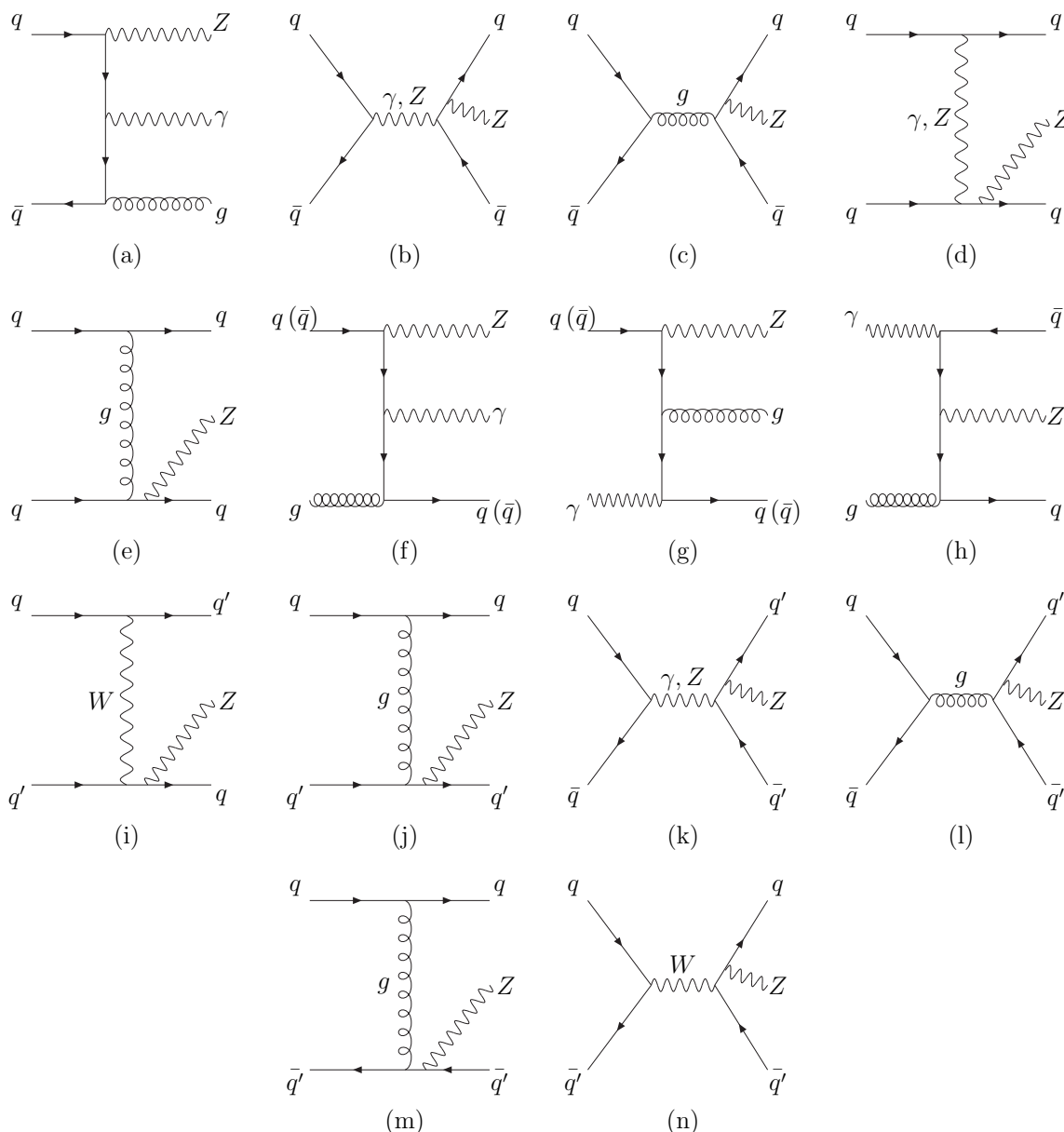


Figure 5. Examples of Feynman Diagrams contributing to the double real corrections to the production of a Z boson in hadronic collisions, eqs. (2.13).

2.2.1 Classification of the radiative corrections

The $\mathcal{O}(\alpha)$ and $\mathcal{O}(\alpha\alpha_s)$ corrections can be organised in a gauge invariant way into a photonic and two weak subsets. The photonic subset (Δ_γ) contains all contributions involving a photon i.e. a virtual photon in the loop or a real-emitted photon or a photon-initiated channel; at $\mathcal{O}(\alpha\alpha_s)$ these are dubbed QCD-QED corrections. The first weak subset (Δ_Z) contains contributions from an additional Z boson, either in the loop or as the intermediate propagator in the tree diagrams of double-real contributions. The other weak subset (Δ_W) contains contributions from one or two W bosons and includes Feynman diagrams with a

non-abelian trilinear gauge boson vertex. This subdivision makes the computation, especially the mass factorisation, more organised and is useful for several intermediate checks.

2.2.2 Ultraviolet renormalisation

The prediction of the hadron-level cross section requires to express the bare couplings and masses in terms of physical parameters via renormalisation. The choice of the background field gauge (BFG) [44] allows to restore the validity of $U(1)_{em}$ -like Ward identities between the vertex corrections and the external quark wave function corrections in the full EW model. We explicitly verify these Ward identities at $\mathcal{O}(\alpha)$ and $\mathcal{O}(\alpha\alpha_s)$. We observe at $\mathcal{O}(\alpha)$ that the sum of the photonic correction in the vertex and external quark wave function corrections is UV finite. The same holds for the corrections with the exchange of one virtual Z boson and, separately, for those with one or two W bosons. An identical pattern takes place at $\mathcal{O}(\alpha\alpha_s)$. We are thus left with the discussion of the charge and external gauge boson wave function renormalisation.

If we choose to express (g, g', v) , the $SU(2)_L$ and $U(1)_Y$ couplings and the Higgs field vacuum expectation value, in terms of (G_μ, m_W, m_Z) (dubbed G_μ -scheme), where G_μ is the Fermi constant, then the weak charge renormalisation is achieved by the replacement

$$\frac{g_0}{c_0} Z_{ZZ}^{1/2} \rightarrow \sqrt{4\sqrt{2}G_\mu m_Z^2} \left(1 - \frac{1}{2}\Delta r + \frac{1}{2}\delta g_Z\right). \quad (2.14)$$

We denote with a 0 subscript all the bare quantities.

We abbreviate with $c_W = m_W/m_Z$ the cosine of the weak mixing angle ($s_W^2 = 1 - c_W^2$), and we define

$$\begin{aligned} \delta e &= e_0 - e, & \delta m_{W,Z}^2 &= m_{W,Z}^2 - m_{W,Z}^2 \\ \delta s_W^2 &= c_W^2 \left(\delta m_Z^2/m_Z^2 - \delta m_W^2/m_W^2\right) \\ \delta g_Z &\equiv \delta Z_{ZZ} + \delta e^2/e^2 + (s_W^2 - c_W^2)/(c_W^2)(\delta s_W^2/s_W^2) \end{aligned}$$

where $Z_{ZZ} = 1 + \delta Z_{ZZ}$ is the ZZ wave function renormalisation constant, δe and $\delta m_{W,Z}$ are the electric charge and gauge boson mass counterterms, respectively. The symbol δs_W^2 is introduced for convenience, but it does not represent an independent counterterm. Δr is a finite correction [45] expressing the relation between the Fermi constant and the muon decay amplitude. The δg_Z factor is, in the BFG, an UV finite correction and this fact yields a considerable simplification in the study of the impact of different input schemes. The Δr parameter and the counterterms can be evaluated in perturbation theory and we keep terms of $\mathcal{O}(\alpha)$ and $\mathcal{O}(\alpha\alpha_s)$ [46, 47]. For consistency, they have to be expressed in terms of (G_μ, m_W, m_Z) . In addition to the redefinition of the overall weak coupling, a second renormalisation correction modifies the vector coupling v_q of the Z boson to the quarks: $v_q = T_3^{(q)} - 2Q_q s_W^2 \rightarrow T_3^{(q)} - 2Q_q (s_W^2 + \delta s_W^2 + (c_W s_W/2) \delta Z_{AZ})$, with δZ_{AZ} the renormalisation constant of the $\gamma - Z$ mixing. In the BFG also this shift of v_q is UV finite.

If we instead choose to relate (g, g', v) to the (α, m_W, m_Z) set of inputs (dubbed $\alpha(0)$ -scheme), the replacement of the overall coupling is $g_0/c_0 Z_{ZZ}^{1/2} \rightarrow \sqrt{4\pi\alpha}/(s_W c_W) \left(1 + \frac{1}{2}\delta g_Z\right)$, while the redefinition of the vector coupling remains the same as in the other scheme.¹

¹An alternative input scheme, convenient to parameterise the Z resonance, has been discussed in ref. [48].

The $\alpha(0)$ -scheme choice is historically [45, 49] one of the simplest EW renormalisation input schemes, but the low scale at which the fine structure constant is measured yields in turn the appearance of large logarithmic corrections in the perturbative expansion. The results depend on the value of the light-quark masses or, alternatively, on an experimental input $\Delta\alpha_{\text{had}}(m_Z) = 4\pi \left(\Pi_{\gamma\gamma}^{(5)}(m_Z^2) - \Pi_{\gamma\gamma}^{(5)}(0) \right)$ [50–53] needed to evaluate the hadronic contribution to the running of the electromagnetic coupling at low scales, where $\Pi_{\gamma\gamma}^{(5)}(q^2)$ indicates the contribution of the first five light quark flavors to the photon vacuum polarisation at a scale q^2 (cfr. ref. [47]).

2.2.3 Infrared singularities and mass factorisation

Each UV-renormalised process, eqs. (2.11)–(2.13), is in general IR divergent, because of the exchange of a soft and/or collinear gluon or photon. Thanks to the KLN theorem, after combining all the partonic subprocesses and summing over all degenerate states, only initial-state collinear singularities are left. The latter are absorbed in the definition of the physical proton PDFs, by means of the mass factorisation kernel Γ . The subtraction kernels at $\mathcal{O}(\alpha\alpha_s)$ are based on the splitting functions computed in ref. [54]. The photonic initial-state collinear singularities are reabsorbed in the definition of the physical proton PDFs and are resummed to all orders via the DGLAP evolution of the parton densities with a QED kernel. The consistent evaluation at $\mathcal{O}(\alpha\alpha_s)$ of the hadron-level cross section requires a proton PDF set featuring DGLAP QED evolution, and, as already presented in eq. (2.3), the inclusion of photon-induced subprocesses.

3 Computational details

In this section we present the details of the calculation. We first introduce our general strategy, which is based on the conversion of all the phase-space integrals into loop integrals, using the so-called reverse unitarity approach. We then discuss in detail the challenges posed by some new MIs with internal massive lines. We eventually provide a detailed account of how we deal with the appearing elliptic integrals.

3.1 General strategy

The evaluation of the partonic cross-sections beyond LO requires the computation of Feynman loop integrals from virtual diagrams as well as two- and three-particle phase-space integrals arising from real emissions. In the very beginning of inclusive NNLO calculations, the phase-space integrals were performed using parametric and angular integration. However, to benefit from state-of-the-art techniques, developed for virtual integrals, we use the method of reverse unitarity [55, 56] to convert the phase-space integrals into loop integrals. The reverse unitarity technique relies on the fact that the following replacement, Cutkosky rule,

$$\delta(p^2 - m^2) \rightarrow \frac{1}{2\pi i} \left(\frac{1}{p^2 - m^2 + i0_+} - \frac{1}{p^2 - m^2 - i0_+} \right) \quad (3.1)$$

allows to convert the Dirac delta function in the phase-space measure of each final state particle into the difference of two propagators with opposite prescriptions for their imaginary

part, where 0_+ is an infinitesimal positive real number. The resulting integrals can then be studied with the help of standard techniques for virtual integrals, like integration-by-parts (IBP) identities and the method of differential equations. The latter require the knowledge of the boundary condition (BC) values to fix the general solution of the problem, and the BCs in turn must be computed as regular phase-space integrals. We comment at the end of the section about the different techniques adopted to compute the BCs.

The amplitudes that one needs to calculate can be classified as follows: two-loop $2 \rightarrow 1$ virtual amplitudes and two-loop $2 \rightarrow 2$ forward-scattering amplitudes with two- or three-particle cuts, stemming from the real-virtual and double-real corrections, respectively. There are up to two internal masses, which are in general complex valued. Once the Feynman diagrams contributing to these processes are generated using tools like QGRAF [57] or FEYNARTS [58], we compute the interference with the corresponding tree-level. We use in-house FORM [59] or MATHEMATICA codes for this algebraic part of the computation. The interference term is expressed in terms of a large number of scalar integrals, that are not all independent, evaluated in d space-time dimensions. Dimensionally regularised scalar integrals satisfy IBP identities [60–62]. These identities link different scalar integrals with each other and make possible the reduction of a large number of terms to a small set of independent quantities, called the MIs. For the IBP reduction process, we have used the public programs KIRA [63], LITERED [64, 65] and REDUZE2 [66, 67].

The EW corrections entail the presence of masses in the loop propagators, specifically m_Z and m_W . Accordingly, the integrals that have to be evaluated depend, in general, on three scales (or two dimensionless ratios). The fact that the two masses are numerically very close to each other can be used to reduce, effectively, the number of scales in the loop integrals, minimising the complexity of the calculation of the MIs. In fact, we can conveniently express the W boson squared mass as

$$m_W^2 = m_Z^2 (1 - \xi), \quad \text{with} \quad \xi = 1 - \frac{m_W^2}{m_Z^2} \simeq 0.2. \quad (3.2)$$

This makes it possible to expand the loop integrands, which contain m_W^2 , as a Taylor series in the parameter ξ . Thus, loop integrals will only depend on \hat{s} and m_Z^2 , hence z , and the dependence on m_W^2 is formally confined into the coefficients of those integrals. The Taylor expansion in ξ will generate loop propagators with higher powers, the so-called dotted propagators, without affecting the topology of the diagrams. Therefore, the set of MIs will not change. The number of terms of such power expansion that have to be retained depends on the phenomenological accuracy we need for the evaluation of the corrections. After IBP reduction, the generic structure of the squared matrix element integrated over the inclusive phase space will then be

$$\int d\Phi |\mathcal{M}|^2 = \sum_{k=1}^N \sum_{j=0}^n \xi^j c_{k,j}(z, d) I_k(z, d), \quad (3.3)$$

where the $c_{k,j}$ are rational functions of the kinematical invariant z and the number d of space-time dimensions, while the $I_k(z, d)$ are the N MIs of the process. In this work, we

have considered only up to the $n = 2$ order in the ξ expansion² and we will discuss the impact of this truncation in section 5.

The following step is to evaluate the MIs as a function of z and d . We use the method of differential equations [68–75] to solve the MIs. We differentiate one MI with respect to z and we use the IBP identities on the differentiated output to express it as a combination of the MI itself and of other MIs. Applying this procedure on all the MIs of an integral family, we obtain a system of first-order linear differential equations, which can be solved given a set of BCs. In the current calculation the differential equations for most of the MIs, can be solved expressing the solution in terms of harmonic polylogarithms (HPLs), generalised harmonic polylogarithms³ (GPLs) [76–79] and cyclotomic HPLs [80]. Three MIs in the evaluation of the double-real corrections, need elliptic extensions of such functions, known as elliptic polylogarithms.

3.2 Evaluation of the full set of master integrals

The MIs which appear in the reduction of the squared matrix element of the different partonic subprocesses can be classified in three groups associated to the two-loop virtual corrections, the two-particle phase-space integrals of the real-virtual corrections and the three-particle phase-space integrals of the double-real processes. All the two-loop virtual MIs were already available in the literature [81–88]. We recompute them using the method of differential equations, starting with a generic off-shell value of the Z boson virtuality and then taking the on-shell limit of the results. The latter are expressed in terms of multiple zeta values and cyclotomic constants [80], which can be reduced to a set of independent constants as introduced in [89]. The off-shell virtual integrals and most of their on-shell limits have been independently checked using FIESTA [90].

In the real-virtual and double-real corrections, the MIs with only massless internal lines were available from ref. [56]. The new MIs with internal massive lines in real-virtual and double-real contributions are solved by employing again the differential equations technique. In these systems of differential equations, square root letters appear, making a direct solution cumbersome. To solve this problem, it is customary to perform a change of variables and to rationalize the square root factors. The presence, in some of the MIs under study, of multiple square roots makes it impossible to rationalize all the letters with one single variable transformation. In these cases, we exploit the linearity property of the integral operator and divide the MI into two (or more) subsystems. At this stage, we can choose for each subsystem a different transformation rule which rationalizes its specific letters. We trade the explicit dependence on z of the full solution with the one on several new kinematical variables, but we obtain a simpler representation of the solution in terms of a compact alphabet as presented later in eq. (4.2).

²While for the evaluation of the MIs involved in the real-virtual and double real corrections such an expansion is indeed needed, the virtual corrections can be evaluated keeping the full dependence on m_Z and m_W , as discussed in section 4.2.

³Note that our definition of HPL with a positive letter is the GPL with a change of sign e.g. $H_1(z) = -G_1(z)$, $H_{i_1}(z) = -G_{i_1}(z)$.

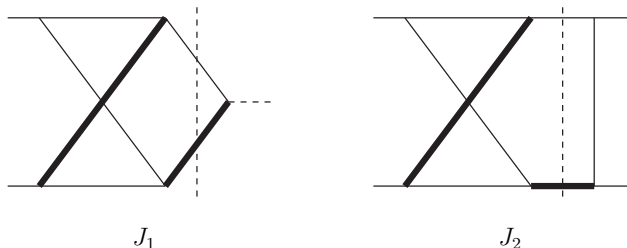


Figure 6. Two MIs, J_1 and J_2 , for the real-virtual corrections. Thin plain lines represent massless particles, while thick plain lines represent massive particles.

Some of the MIs of the present study satisfy coupled differential equations and the problems of rationalising the letters and decoupling the equations are intertwined. We describe in the following example how the two issues can be simultaneously handled.

3.2.1 Example: a subsystem of two real-virtual master integrals

We consider two integrals $J_1 \equiv J_1(z)$ and $J_2 \equiv J_2(z)$ (see figure 6), which satisfy the following system of differential equations:

$$\begin{aligned} J_1' &= \frac{4(d-3)z^2 - d + 6}{z(1+4z^2)} J_1 + r_1(d, z), \\ J_2' &= \frac{2}{z} J_2 + \frac{(2d-9)(2z+1)}{4z^2+1} J_1 + r_2(d, z). \end{aligned} \tag{3.4}$$

The functions $r_{1,2}$ are the inhomogeneous part of the equations and contain rational functions and GPLs. With the transformation rule

$$z \rightarrow \frac{w}{1-w^2} \tag{3.5}$$

and the relations

$$\begin{aligned} H_0(z) &= H_0(w) + H_1(w) - H_{-1}(w), \\ H_1(z) &= H_{i_1}(w) - H_{-i_2}(w) - H_1(w) + H_{-1}(w) \end{aligned} \tag{3.6}$$

the first differential equation of eq. (3.4) can be rationalised and, with appropriate boundary conditions, can be solved to obtain up to $\mathcal{O}(\varepsilon^{-1})$ as

$$\begin{aligned} J_1^{(-2)} &= 0, \\ J_1^{(-1)} &= \frac{w^2}{1-w^4} \left(i\pi(3H_0(w) + H_1(w) + H_{-1}(w)) - 7H_{0,0}(w) - 4H_{0,1}(w) + 3H_{0,-i_2}(w) \right. \\ &\quad \left. - 3H_{0,i_1}(w) + 4H_{0,-1}(w) - H_{1,0}(w) - H_{1,i_1}(w) - H_{-1,0}(w) - H_{-1,i_1}(w) + 3\zeta_2 \right. \\ &\quad \left. + H_{1,-i_2}(w) + H_{-1,-i_2}(w) \right). \end{aligned}$$

This allows us to readily obtain the solution for $J_2^{(-2)}$. However, the differential equation for $J_2^{(-1)}$ has contributions to its non-homogeneous part from $r_2^{(-2)}, r_2^{(-1)}, J_2^{(-2)}$ as well as

$J_1^{(-1)}$. The transformation rule in eq. (3.5) does not rationalize the former contributions, but it rather converts the linear kernels to much more involved polynomials. At this point the difficulty of solving the system for $J_{1,2}$ is evident, as cumbersome letters would appear in the GPLs, making the next integrations impossible. We reorganize the problem with the working hypothesis that, at two-loop level, all the coefficients of the poles in ε are expressible in terms of simple GPLs. In other words we expect to be able to find a combination of $J_1^{(n)}$ and $J_2^{(n)}$ such that their single pole can still be determined with elementary integrations.

With this goal, we define a new integral J_0

$$J_0^{(n)} = \left(z - \frac{1}{2}\right) J_1^{(n)} + J_2^{(n)} \tag{3.7}$$

and we observe that $J_0^{(-1)}$ satisfies a linear differential equation independent of both $J_1^{(-1)}$ and $J_2^{(-1)}$. We solve it and obtain

$$\begin{aligned} J_0^{(-2)} &= z^2(H_0(z) + H_1(z) - i\pi), \\ J_0^{(-1)} &= -\frac{z^2}{2} \left(2H_{\frac{1}{2},0}(z) + 2H_{\frac{1}{2},1}(z) - 7H_{0,0}(z) - 7H_{0,1}(z) - 10H_{1,0}(z) - 10H_{1,1}(z) \right. \\ &\quad \left. + i\pi(2\ln(2) + 3H_0(z) + 4H_1(z)) \right). \end{aligned} \tag{3.8}$$

Consistently replacing each $J_2^{(n)}$ using eq. (3.7), both in the system of differential equations and in the matrix elements, we also remove the dependence of $J_1^{(0)}$. However, the contribution from $J_1^{(-1)}$, can not be eliminated, as expected. Hence, the issue of rationalisation remains in the full non-homogeneous part of $J_0^{(0)}$. The non-homogeneous part of $J_0^{(0)}$ can be split in the sum of two terms, with or without a relation with the square root letter: we use the change of variables to w to linearise only for the former, while we keep the variable z for the latter. When we solve the non-homogeneous equation, we consider two separate integrals, with the integrand functions depending only on w or only on z , with straightforward results in terms of GPLs, in the following form

$$\begin{aligned} J_0^{(0)} &= z^2 \left(-9\zeta_3 + \dots - 2H_{\frac{1}{2},\frac{1}{2},0}(z) - 2H_{\frac{1}{2},\frac{1}{2},1}(z) - 5H_{\frac{1}{2},0,0}(z) - 6H_{\frac{1}{2},0,1}(z) \right. \\ &\quad \left. + 19H_{1,1,1}(z) + \dots \right) + \frac{w^2}{(1-w^2)^2} \left(-3H_{-1}(w)\zeta_2 + \dots + H_{1,-1,0}(w) + 3H_{1,0,i_1}(w) \right. \\ &\quad \left. - 3H_{1,0,-i_2}(w) + \dots \right). \end{aligned} \tag{3.9}$$

The absence of the square root in the letters allows a smooth numerical evaluation. In the previous example, we find that a certain combination of MIs can be helpful to avoid the appearance of “complicated” GPLs in the intermediate steps of the solution of the system, under the assumption that they are not expected in the coefficients of the poles in ε . This remark simplifies in turn the solution of the system for the finite part of the MIs. For example, the contributions from $J_1^{(0)}$ and $J_2^{(0)}$ do individually contain the problematic GPLs, which however would eventually cancel in the final result. Our direct evaluation of $J_0^{(0)}$ instead avoids these GPLs from the very beginning.

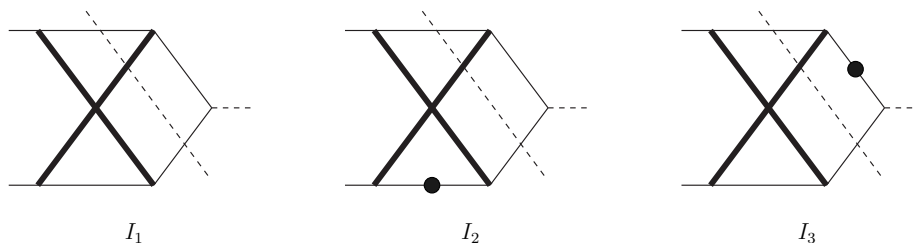


Figure 7. The three elliptic MIs, I_1 , I_2 and I_3 , contributing to the real-virtual corrections. Thin plain lines represent massless particles, while thick plain lines represent massive particles. A dot on a line represents the squared propagator.

Apart from the square root letters, we also find three MIs in the double-real corrections for which the coupled sub-system of differential equations can not be factorised to first order, indicating that the MIs contain elliptic polylogarithms. In the next sub-section we present the details of the computation of these MIs.

3.2.2 Solving the master integrals with elliptic kernels

The double real corrections receive contributions from scattering processes with quark and anti-quark both in the initial and final state, whose matrix elements include contributions with the exchange of either an EW boson or a gluon. The interference of these two terms is of $\mathcal{O}(\alpha\alpha_s)$ and is relevant to our calculation. In these interferences, a non-trivial topology gives rise to three MIs $\{I_1, I_2, I_3\}$ (see figure 7) which are of elliptic kind. The 3×3 system of differential equations is not first-order factorizable. The homogeneous part of the system is given in each order of ε as

$$d_z \begin{pmatrix} I_1^{(n)} \\ I_2^{(n)} \\ I_3^{(n)} \end{pmatrix} = \begin{bmatrix} \frac{4}{3z} & -\frac{2}{3z} & \frac{2}{3} \frac{1}{z^2} \\ \frac{4}{3(1+8z)} & \frac{-3-31z+16z^2}{3(-1+z)z(1+8z)} & \frac{2(5+4z)}{3(-1+z)z(1+8z)} \\ -\frac{2}{3(1+8z)} & \frac{5+4z}{3(-1+z)(1+8z)} & \frac{-11-46z+48z^2}{3(-1+z)z(1+8z)} \end{bmatrix} \begin{pmatrix} I_1^{(n)} \\ I_2^{(n)} \\ I_3^{(n)} \end{pmatrix} + \begin{pmatrix} R_1^{(n)} \\ R_2^{(n)} \\ R_3^{(n)} \end{pmatrix}.$$

The homogeneous part of this system of equations is the same as the one studied for the corresponding virtual diagrams in refs. [86, 91]. In those papers, the results are obtained in terms of elliptic integrals of the first kind and eMPLs, respectively. The current system can be solved order-by-order in ε , and we expect to find only standard HPLs in the poles, while eMPLs will appear in the finite parts and higher orders in ε .

Formally, since the IBP reduction introduces a $1/\varepsilon$ factor in the coefficient of these integrals in the matrix elements, then we would need to evaluate $I_{1,2,3}$ up to $\mathcal{O}(\varepsilon)$, in order to compute all the finite corrections. For the same argument, we expect that individual contributions to the coefficient of the single pole of the matrix elements are expressed via eMPL. We formulate a physical Ansatz as in the previous section, imposing the simpler polylogarithmic structure of the single pole of the matrix element, i.e. the absence of eMPLs in its final expression. We thus find the following combination of the elliptic MIs,

$$I_0^{(n)} = z(1 + 2z)I_1^{(n)} + z(1 - 4z)I_2^{(n)} - (1 + 5z)I_3^{(n)}. \tag{3.10}$$

The differential equation of $I_0^{(-1)}$ and $I_0^{(0)}$ turns out to be linear and independent of $I_1^{(0)}$, $I_2^{(0)}$ and $I_3^{(0)}$. We solve it to obtain the following solution:

$$\begin{aligned}
 I_0^{(-1)} &= \frac{1}{2}z^2(-1+4z)H_0(z), \\
 I_0^{(0)} &= \left(-\frac{5z^2}{2} + \frac{6z^4}{-1+z}\right)H_{0,0}(z) + 2z^2(-1+4z)H_{0,1}(z) + 2(1-4z)z^2\zeta_2. \quad (3.11)
 \end{aligned}$$

This new combination of MIs explicitly exhibits the absence of eMPL in their single pole and allows in turn a straightforward check of the pole cancellations in the cross section. Clearly, since the combination $I_0^{(1)}$ does not remain independent of $I_2^{(0)}$, $I_3^{(0)}$ we find eMPLs contributing to the finite part of the matrix elements. For the numerical evaluation, a series representation of the integrals is equivalent to the formal solution via eMPLs. Hence, we solve $I_2^{(0)}$ and $I_3^{(0)}$ in Taylor series expansion around $z = 0, 1/2, 1$. (See for instance [86, 92–97]). $I_2^{(0)}$ and $I_3^{(0)}$ are regular in the whole range of z , while $I_0^{(1)}$ instead contains logarithmically enhanced terms. The latter yield a singular behaviour at a point which does not correspond to any physical threshold. These logarithms are thus expected to cancel against analogous terms stemming from other MIs. In order to achieve an exact analytical cancellation, we further elaborate the solution of $I_0^{(1)} \equiv I_{\text{ell}}^{(0,1)} = I_0^{(1.HPL)} + \delta_{\text{ell}}^{(0,1)}$, by splitting its expression in two parts: one with the closed form of the logarithmic dependence and one regular remainder given via a Taylor expansion. We obtain

$$\begin{aligned}
 I_{\text{ell}}^{(0,1)} &= -35z^3H_{-\frac{1}{2},0,0}(z) - 60z^3H_{-\frac{1}{2},0,1}(z) + \frac{1}{2}z^2(-3 + 86z - 24z^2\bar{z})H_{0,0,0}(z) - 2z^2(5 \\
 &\quad - 35z + 42z^2)\bar{z}H_{0,0,1}(z) - 2z^2(2 - 12z + 7z^2)\bar{z}H_{0,1,0}(z) - 8(1 - 4z)z^2H_{0,1,1}(z) \\
 &\quad - 4z^2(1+z)(2+z)\bar{z}H_{0,-1,0}(z) - 2z^2(1-3z+8z^2)\bar{z}H_{1,0,0}(z) + 60z^3H_{-\frac{1}{2}}(z)\zeta_2 \\
 &\quad + 6z^2(1-12z+14z^2)\bar{z}H_0(z)\zeta_2 + 2z^3(-43+49z)\bar{z}\zeta_3 + \delta_{\text{ell}}^{(0,1)}. \quad (3.12)
 \end{aligned}$$

$\delta_{\text{ell}}^{(0,1)}$ has been obtained in Taylor series expansion. In the following, we present $\delta_{\text{ell}}^{(0,1)}$ for the expansion around $y = 1 - z = 0$ and $z = 0$.

$$\begin{aligned}
 \delta_{\text{ell}}^{(0,1)} &= z^3 \left(35H_{-\frac{1}{2},0,0}(1) + 60H_{-\frac{1}{2},0,1}(1) - 60H_{-\frac{1}{2}}(1)\zeta_2 \right. \\
 &\quad \left. - 20y^2 - \frac{1205y^3}{54} - \frac{1535y^4}{72} + \left(10y^2 + \frac{130y^3}{9} + \frac{295y^4}{18} \right) H_0(y) + \mathcal{O}(y^5) \right), \\
 &= 90z^4 - 360z^5 + \frac{21745z^6}{9} - 10z^4(-3 - 6z + 29z^2)H_0(z) - 30z^4(7 - 29z \\
 &\quad + 198z^2)H_{0,0}(z) - 45z^3(-1 - 12z^2 + 72z^3)H_{0,0,0}(z) + (60z^4 - 510z^5 + 3860z^6 \\
 &\quad + 360z^5(-1 + 6z)H_0(z))\zeta_2 + 20z^3(-1 - 27z^2 + 162z^3)\zeta_3 + \mathcal{O}(z^7). \quad (3.13)
 \end{aligned}$$

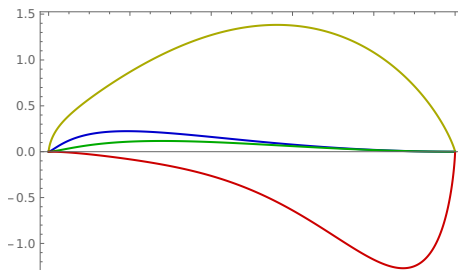


Figure 8. The ε^0 coefficient of the elliptic MIs i.e. $I_1^{(0)}$, $I_2^{(0)}$ and $I_3^{(0)}$ are presented in blue, yellow and green, respectively. The $I_0^{(1)} 10^{-1}$ is shown in red.

$I_2^{(0)} \equiv I_{\text{ell}}^{(2,0)}$ and $I_3^{(0)} \equiv I_{\text{ell}}^{(3,0)}$ are obtained in the two series expansions as follows

$$\begin{aligned}
 I_{\text{ell}}^{(2,0)} &= 3y - \frac{9y^2}{4} - \frac{13y^3}{36} - \frac{7y^4}{72} + \left(-2y + y^2 + \frac{y^3}{3} + \frac{y^4}{6} \right) H_0(y) + \mathcal{O}(y^5), \\
 &= \frac{3}{4} z H_0(z)^2 - 2z^2 (-2 + 3H_0(z)) + z^3 \left(-2(4 + 12\zeta_2 + 9\zeta_3) - 3(-5 + 4\zeta_2) H_0(z) \right. \\
 &\quad \left. + 18H_0(z)^2 + 3H_0(z)^3 \right) + z^4 \left(\frac{8}{9} (122 + 243\zeta_2 + 162\zeta_3) + 2(-55 + 48\zeta_2) H_0(z) \right. \\
 &\quad \left. - 162H_0(z)^2 - 24H_0(z)^3 \right) + z^5 \left(\frac{1}{4} (-3671 - 7416\zeta_2 - 5184\zeta_3) \right. \\
 &\quad \left. - 24(-35 + 36\zeta_2) H_0(z) + \frac{2781}{2} H_0(z)^2 + 216H_0(z)^3 \right) + \mathcal{O}(z^6). \tag{3.14}
 \end{aligned}$$

$$\begin{aligned}
 I_{\text{ell}}^{(3,0)} &= \frac{y^2}{2} - \frac{y^3}{4} - \frac{5y^4}{48} + \mathcal{O}(y^5), \\
 &= z^2 (2H_0(z)^2 - 2\zeta_2) + z^3 (6 + 18\zeta_2 + 18\zeta_3 + (-6 + 12\zeta_2) H_0(z) - 13H_0(z)^2 \\
 &\quad - 3H_0(z)^3) + z^4 \left(-\frac{3}{2} (53 + 100\zeta_2 + 72\zeta_3) - 3(-17 + 24\zeta_2) H_0(z) + 113H_0(z)^2 \right. \\
 &\quad \left. + 18H_0(z)^3 \right) + z^5 \left(\frac{1}{12} (7379 + 14256\zeta_2 + 10368\zeta_3) + \frac{1}{2} (-859 + 1152\zeta_2) H_0(z) \right. \\
 &\quad \left. - \frac{1781}{2} H_0(z)^2 - 144H_0(z)^3 \right) + \mathcal{O}(z^6). \tag{3.15}
 \end{aligned}$$

The series expanded $\delta_{\text{ell}}^{(0,1)}$, $I_2^{(0)}$ and $I_3^{(0)}$, are all regular and admit a Taylor expansion with fast convergence. This procedure provides a series representation of the elliptic functions present in the calculation. In figure 8, we present the numerical evaluation of the elliptic MIs for the whole range of z .

One of the important steps in solving the differential equations of the MIs, is to obtain the BCs. In the case of the two-loop virtual integrals, we obtain the BCs in two ways: by demanding regular behaviour in the limit $z \rightarrow -1$ for the one-mass integrals or $s \rightarrow 0$ for the two-mass integrals; alternatively, by an exact computation in one of these limits. In the case of the phase-space integrals, we have performed the exact phase-space integration

for the MIs which contain only massless internal lines⁴ in the soft limit ($z \rightarrow 1$), and found perfect agreement with the literature [55, 56]. For the double-real emissions, we have followed the parameterisation presented in [56], which has also allowed us to drop the contributions from the massive line/s in the soft limit; we have in turn obtained the BCs of the MIs involving a massive line in terms of the BCs of [55, 56]. For the real-virtual integrals, we have anticipated a few approaches to obtain the BCs. For the simpler MIs, we have computed the one-loop integrals in exact form in z and d , have taken the soft limit ($z \rightarrow 1$), and performed the phase-space integration. For some MIs, we have studied the IBP reduction rules for a “harder” integral, which has provided us the BCs for the MIs under consideration in terms of other, already known, MIs.

4 Analytical results

In this section we present our results. First, we introduce all the variables which appear in our calculation and several other necessary definitions. We then present the analytic finite partonic coefficients $\Delta_\gamma^{(1,1)}$, $\Delta_Z^{(1,1)}$ and $\Delta_W^{(1,1)}$.

4.1 Preliminaries: variables, functions and abbreviations

The partonic cross-section for the production of a Z boson, integrated over the phase-space of the additional emitted partons, depends on the variables s , m_Z and m_W and on the top quark and Higgs boson masses m_t and m_H respectively only through UV renormalisation. As described in section 3.1, we expand the virtual EW amplitudes containing W bosons according to eq. (3.2). For the purpose of clarity and compactness, we present here only results for the $n = 0$ term in the ξ expansion, i.e. $m_W^2 = m_Z^2$.

The Feynman integrals have a rich structure due to the presence of different internal thresholds. When the solution is given in terms of polylogarithmic functions, the internal structure of the integrals is displayed by the values of the weights and of the independent variable of the polylogarithms. The singular or branching points of the solutions are expressed in terms of a set of monomials, the letters, forming an alphabet. The presence in the letters of square-roots, also at multiple levels, can be avoided by appropriate transformations which rationalise the initial expressions. In the current calculation we adopt the following changes of variables:

$$z = \frac{t}{(1+t)^2} = \frac{\rho}{(1-\rho+\rho^2)} = \frac{w}{1-w^2}. \quad (4.1)$$

After these manipulations, the resulting alphabet of the problem is given by:

$$\left\{ -1, -\frac{1}{2}, 0, \frac{1}{2}, 1, \{3, 0\}, \{3, 1\}, \{4, 1\}, \{6, 0\}, \{6, 1\}, i_1, -i_2 \right\}. \quad (4.2)$$

The set $\{-1, 0, 1\}$ is the well-known alphabet for HPLs. $\{\{3, 0\}, \{3, 1\}, \{4, 1\}, \{6, 0\}, \{6, 1\}\}$ denotes the third-, fourth- and sixth-root of unity, which defines the cyclotomic HPLs. The

⁴Apart from the produced Z boson.

set $\{\{4, 1\}, i_1, i_2\}$ appears in a group of diagrams expressed in terms of GPLs, where i_1 and i_2 are given by

$$i_1 = \frac{\sqrt{5}-1}{2} \equiv 0.618034\dots, \quad i_2 = \frac{\sqrt{5}+1}{2} \equiv 1.618034\dots \quad (4.3)$$

We enlist all our definitions below

$$\begin{aligned} H_{-1}(z) &= \int_0^z \frac{dx}{1+x}, & H_0(z) &= \int_0^z \frac{dx}{x}, & H_1(z) &= \int_0^z \frac{dx}{1-x}, \\ H_{-\frac{1}{2}}(z) &= \int_0^z \frac{dx}{\frac{1}{2}+x}, & H_{\frac{1}{2}}(z) &= \int_0^z \frac{dx}{\frac{1}{2}-x}, \\ H_{\{3,0\}}(z) &= \int_0^z \frac{dx}{1+x+x^2}, & H_{\{3,1\}}(z) &= \int_0^z \frac{x dx}{1+x+x^2}, \\ H_{\{6,0\}}(z) &= \int_0^z \frac{dx}{1-x+x^2}, & H_{\{6,1\}}(z) &= \int_0^z \frac{x dx}{1-x+x^2}, \\ H_{\{4,1\}}(z) &= \int_0^z \frac{x dx}{1+x^2}, & H_{i_1}(z) &= \int_0^z \frac{dx}{i_1-x}, & H_{-i_2}(z) &= \int_0^z \frac{dx}{i_2+x}. \end{aligned} \quad (4.4)$$

In order to present the results in compact form, we introduce the following abbreviations for all the polynomials which appear in the denominator of the expressions:

$$\bar{z} \equiv \frac{1}{1-z}, \quad \bar{\bar{z}} \equiv \frac{1}{1-2z}, \quad \hat{\bar{z}} \equiv \frac{1}{1-4z}, \quad \tilde{z} \equiv \frac{1}{1+z}, \quad \tilde{\tilde{z}} \equiv \frac{1}{1+2z}, \quad \hat{\tilde{z}} \equiv \frac{1}{1+4z}, \quad (4.5)$$

$$\bar{t} \equiv \frac{1}{1-t}, \quad \tilde{t} \equiv \frac{1}{1+t}, \quad \hat{t} \equiv \frac{1}{1+t^2}, \quad \check{t} \equiv \frac{1}{1+t+t^2}, \quad (4.6)$$

$$\bar{w} \equiv \frac{1}{(1-w^2)^2}, \quad \tilde{w} \equiv \frac{1}{(1-w^4)}, \quad (4.7)$$

$$\bar{\rho} \equiv \frac{1}{(1-\rho)}, \quad \hat{\rho} \equiv \frac{1}{(1-\rho+\rho^2)}. \quad (4.8)$$

The soft-collinear (plus) distributions are defined as

$$\mathcal{D}_n = \left[\frac{\log^n(1-z)}{(1-z)} \right]_+. \quad (4.9)$$

4.2 The virtual corrections

In this section we present the results for the sole virtual corrections. The two-loop Feynman diagrams contributing to the renormalised $q\bar{q}Z$ vertex are shown in figure 3. We consider the interference with the tree-level and we express it in perturbative expansion of α and α_s as follows

$$\begin{aligned} F &= 1 + \frac{\alpha_s}{4\pi} F^{(1,0)} + \frac{\alpha}{4\pi} \left(F_\gamma^{(0,1)} + \frac{1}{s_W^2 c_W^2} F_Z^{(0,1)} + \frac{1}{s_W^2} F_W^{(0,1)} \right) \\ &+ \frac{\alpha}{4\pi} \frac{\alpha_s}{4\pi} \left(F_\gamma^{(1,1)} + \frac{1}{s_W^2 c_W^2} F_Z^{(1,1)} + \frac{1}{s_W^2} F_W^{(1,1)} \right) + \dots \end{aligned} \quad (4.10)$$

The photonic contributions are denoted by $F_\gamma^{(m,n)}$ and they have been presented in [31, 98]. Below, we present the renormalised contributions with one Z boson or one/two W boson/s

in the loop, denoted by $F_Z^{(m,n)}$ and $F_W^{(m,n)}$, respectively. We present here the results for the zeroth order in ξ . We have also computed the completely general case with different masses and compared it against the results available in the literature in [88], finding agreement. We have performed the calculation in the background field gauge. Therefore, we have included the sole wave function renormalisation, which is sufficient to obtain UV finiteness. In our expressions, the following constant c_1 [99] appears

$$c_1 = 12\zeta_2 \ln^2(2) + \ln^4(2) + 24\text{Li}_4\left(\frac{1}{2}\right). \quad (4.11)$$

We express the on-shell two-loop virtual integrals through the constants as presented in [89], where G_R and G_I are introduced as

$$G(a_1, \dots, a_w, 1) = G_R(a_1, \dots, a_w) + iG_I(a_1, \dots, a_w). \quad (4.12)$$

G denotes GPLs. r_2 and r_4 are given by

$$r_2 = \frac{1}{2} - i\frac{\sqrt{3}}{2}, \quad r_4 = -\frac{1}{2} - i\frac{\sqrt{3}}{2}. \quad (4.13)$$

The one- and two-loop results for $F_Z^{(m,n)}$ and $F_W^{(m,n)}$, in the case of u -quark initial state, are in order:

$$F_Z^{(0,1)} = c_u^{(4)} \left[-\frac{11}{2} + 4\zeta_2 - i\pi(5 - 8\ln(2)) \right], \quad (4.14)$$

$$\begin{aligned} F_Z^{(1,1)} = C_F c_u^{(4)} & \left[\frac{1}{\epsilon^2} \left\{ 11 - 8\zeta_2 + i\pi(10 - 16\ln(2)) \right\} + \frac{1}{\epsilon} \left\{ 52 - 114\zeta_2 - 38\zeta_3 + 168\zeta_2 \ln(2) \right. \right. \\ & + i\pi(50 - 24\zeta_2 - 28\ln(2) + 8\ln^2(2)) \left. \right\} + 195 - \frac{26c_1}{3} - 436\zeta_2 + \frac{904}{5}\zeta_2^2 - \frac{229}{2}\zeta_3 \\ & + 366\zeta_2 \ln(2) - 24\zeta_2 \ln^2(2) + i\pi \left(261 - 118\zeta_2 - 210\zeta_3 - 38\ln(2) + 168\zeta_2 \ln(2) \right. \\ & \left. \left. + 38\ln^2(2) - \frac{40}{3}\ln^3(2) \right) \right], \quad (4.15) \end{aligned}$$

$$F_W^{(0,1)} = c_u^2 \left(-\frac{7}{8} + \frac{5}{4}\frac{\pi}{\sqrt{3}} - \zeta_2 \right) + c_u c_d \left(-\frac{1}{2} - \frac{5}{4}\frac{\pi}{\sqrt{3}} + 2\zeta_2 - i\pi \left(\frac{5}{4} - 2\ln(2) \right) \right), \quad (4.16)$$

$$\begin{aligned} F_W^{(1,1)} = C_F c_u^2 & \left[\frac{1}{\epsilon^2} \left\{ \frac{7}{4} - \frac{5}{2}\frac{\pi}{\sqrt{3}} + 2\zeta_2 \right\} + \frac{1}{\epsilon} \left\{ \frac{19}{2} - \frac{35}{4}\frac{\pi}{\sqrt{3}} + \frac{5}{2}\ln(3) \frac{\pi}{\sqrt{3}} + 3\zeta_2 - \frac{2}{3}\zeta_3 \right. \right. \\ & - \frac{4}{3}\pi G_I(0, r_2) + 10\frac{1}{\sqrt{3}} G_I(0, r_2) + i\pi \left(\frac{7}{4} - \frac{5}{2}\frac{\pi}{\sqrt{3}} + 2\zeta_2 \right) \left. \right\} + \left\{ \frac{143}{4} - \frac{97}{4}\frac{\pi}{\sqrt{3}} + \frac{67}{6}\zeta_2 \right. \\ & + \frac{55}{9}\frac{\pi}{\sqrt{3}}\zeta_2 - \frac{145}{9}\zeta_2^2 - \frac{1}{3}\zeta_3 - \frac{4}{3}\pi G_I(0, r_2) + \frac{91}{2}\frac{1}{\sqrt{3}} G_I(0, r_2) + \frac{44}{3} G_I(0, r_2)^2 \\ & + 2\pi G_I(0, 1, r_4) + 5\sqrt{3} G_I(0, 1, r_4) + \frac{35}{4}\frac{\pi}{\sqrt{3}} \ln(3) + \frac{2}{3}\pi G_I(0, r_2) \ln(3) \\ & - 5\frac{1}{\sqrt{3}} G_I(0, r_2) \ln(3) - \frac{5}{4}\frac{\pi}{\sqrt{3}} \ln^2(3) + i\pi \left(\frac{75}{2} - \frac{35}{4}\frac{\pi}{\sqrt{3}} + 3\zeta_2 - \frac{74}{3}\zeta_3 \right. \\ & \left. \left. - \frac{4}{3}\pi G_I(0, r_2) + 10\frac{1}{\sqrt{3}} G_I(0, r_2) + \frac{5}{2}\frac{\pi}{\sqrt{3}} \ln(3) \right) \right\} + C_F c_u c_d \left[\frac{1}{\epsilon^2} \left\{ 1 + \frac{5}{2}\frac{\pi}{\sqrt{3}} - 4\zeta_2 \right. \right. \end{aligned}$$

$$\begin{aligned}
 & + i\pi \left(\frac{5}{2} - 4 \log(2) \right) \left. \right\} + \frac{1}{\epsilon} \left\{ \frac{7}{2} + \frac{35}{4} \frac{\pi}{\sqrt{3}} - \frac{63}{2} \zeta_2 - \frac{53}{6} \zeta_3 + \frac{4}{3} \pi G_I(0, r_2) \right. \\
 & - 10 \frac{1}{\sqrt{3}} G_I(0, r_2) + 42 \zeta_2 \log(2) - \frac{5}{2} \frac{\pi}{\sqrt{3}} \log(3) + i\pi \left(\frac{43}{4} + \frac{5}{2} \frac{\pi}{\sqrt{3}} - 8 \zeta_2 - 7 \log(2) \right. \\
 & \left. \left. + 2 \log^2(2) \right) \right\} + \left\{ 13 - \frac{13}{6} c_1 + \frac{97}{4} \frac{\pi}{\sqrt{3}} - \frac{721}{6} \zeta_2 - \frac{55}{9} \pi \frac{\zeta_2}{\sqrt{3}} + \frac{2759}{45} \zeta_2^2 - \frac{679}{24} \zeta_3 \right. \\
 & + \frac{4}{3} \pi G_I(0, r_2) - \frac{91}{2} \frac{1}{\sqrt{3}} G_I(0, r_2) - \frac{44}{3} G_I(0, r_2)^2 - 2\pi G_I(0, 1, r_4) - 5\sqrt{3} G_I(0, 1, r_4) \\
 & + \frac{183}{2} \zeta_2 \ln(2) - 6\zeta_2 \ln^2(2) - \frac{35}{4} \pi \frac{1}{\sqrt{3}} \ln(3) - \frac{2}{3} \pi G_I(0, r_2) \ln(3) \\
 & + 5 \frac{1}{\sqrt{3}} G_I(0, r_2) \ln(3) + \frac{5}{4} \frac{\pi}{\sqrt{3}} \ln^2(3) + i\pi \left(\frac{111}{4} + \frac{35}{4} \frac{\pi}{\sqrt{3}} - \frac{65}{2} \zeta_2 - \frac{167}{6} \zeta_3 \right. \\
 & + \frac{4}{3} \pi G_I(0, r_2) - 10 \frac{1}{\sqrt{3}} G_I(0, r_2) - \frac{19 \ln(2)}{2} + 42 \zeta_2 \ln(2) + \frac{19}{2} \ln^2(2) - \frac{10}{3} \ln^3(2) \\
 & \left. \left. - \frac{5}{2} \frac{\pi}{\sqrt{3}} \log(3) \right) \right\} \left. \right], \tag{4.17}
 \end{aligned}$$

where we defined the following combinations of vector and axial-vector couplings:

$$c_q^{(4)} = C_{v,q}^4 + 6C_{v,q}^2 C_{a,q}^2 + C_{a,q}^4, \tag{4.18}$$

$$c_q = C_{v,q} + C_{a,q}, \tag{4.19}$$

with $C_{v,q}$ and $C_{a,q}$ defined in eq. (2.5) and $q \in (u, d)$.

4.3 The partonic coefficients for QED

The photonic part ($\Delta_\gamma^{(1,1)}$) of the total hadronic cross-section has been defined in eq. (2.7) and receives contributions from several partonic channels which are convoluted with the physical proton PDFs as follows

$$\begin{aligned}
 \Delta_\gamma^{(1,1)} &= \sum_{q \in Q, \bar{Q}} f_q \otimes f_{\bar{q}} \otimes \Delta_{q\bar{q}}^{(1,1)} + \sum_{q \in Q, \bar{Q}} f_q \otimes f_q \otimes \Delta_{qq}^{(1,1)} \\
 &+ \sum_{q \in Q, \bar{Q}} (f_q \otimes f_g + f_g \otimes f_q) \otimes \Delta_{qg}^{(1,1)} + \sum_{q \in Q, \bar{Q}} (f_q \otimes f_\gamma + f_\gamma \otimes f_q) \otimes \Delta_{q\gamma}^{(1,1)} \\
 &+ (f_g \otimes f_\gamma + f_\gamma \otimes f_g) \otimes \Delta_{g\gamma}^{(1,1)}. \tag{4.20}
 \end{aligned}$$

The sums run over all flavours of quarks (q) and antiquarks (\bar{q}). The following combination of vector and axial-vector couplings, along with electric charge, appear in all these partonic channels with a photonic correction:

$$c_q^{(2)} = Q_q^2 (C_{v,q}^2 + C_{a,q}^2). \tag{4.21}$$

In eq. (4.21) q can be an up- or a down-type quark. The partonic cross-section for all the channels are given below. We have set the factorisation scale $\mu_F = m_Z$ in presenting these results.

$$\begin{aligned}
 \Delta_{q\bar{q}}^{(1,1)} = c_q^{(2)} C_F \left\{ \delta(1-z) \left(\frac{511}{2} - 140\zeta_2 + \frac{16}{5}\zeta_2^2 - 120\zeta_3 \right) + 512\zeta_3 \mathcal{D}_0 - \mathcal{D}_1 \left(512 + 256\zeta_2 \right) \right. \\
 + 256\mathcal{D}_3 + \zeta_2 \left(192 - \frac{48}{1-z} - 176z - 96z^2 + \left(16 + \frac{64}{1-z} + 176z + 96z^2 \right) H_0(z) \right. \\
 + \left. \left(-80 - \frac{64}{1-z} - 80z \right) H_1(z) - 96(1+z)^2 H_{-1}(z) \right) + 16\zeta_3 \left(-3 - \frac{20}{1-z} \right. \\
 + 13z + 8z^2 \left. \right) + 448 - 328z - 104z^2 + \left(64 + \frac{320}{1-z} + 152z \right) H_0(z) - 8(32 \\
 + 31z) H_1(z) + \left(96 + \frac{120}{1-z} - 240z^2 \right) H_{0,0}(z) - \left(64 - \frac{96}{1-z} - 288z \right) H_{0,1}(z) \\
 + \left(-48 + \frac{48}{1-z} + 144z - 144z^2 \right) H_{1,0}(z) + 256(-1+z) H_{1,1}(z) \\
 + 96(1+z)^2 H_{-1,0}(z) + \left(184 - \frac{160}{1-z} + 280z + 32z^2 \right) H_{0,0,0}(z) + \left(320 - \frac{448}{1-z} \right. \\
 + 320z \left. \right) H_{0,0,1}(z) + \left(496 - \frac{640}{1-z} + 624z + 64z^2 \right) H_{0,1,0}(z) + \left(624 - \frac{992}{1-z} \right. \\
 + 624z \left. \right) H_{0,1,1}(z) + 64(1+z)^2 H_{0,-1,0}(z) + \left(304 - \frac{416}{1-z} + 304z \right) H_{1,0,0}(z) \\
 + \left(512 - \frac{960}{1-z} + 512z \right) H_{1,0,1}(z) + \left(560 - \frac{1024}{1-z} + 560z \right) H_{1,1,0}(z) \\
 \left. + 768(1+z) H_{1,1,1}(z) + 160(1+z)^2 H_{-1,0,0}(z) - 192(1+z)^2 H_{-1,-1,0}(z) \right\}. \quad (4.22)
 \end{aligned}$$

$$\begin{aligned}
 \Delta_{qg}^{(1,1)} = c_q^{(2)} \left\{ \zeta_2 \left(1 - 20z + 16z^2 + 2(7 - 14z + 24z^2) H_0(z) + 16(1 - 2z + 2z^2) H_1(z) \right) \right. \\
 + \zeta_3 \left(26 - 52z + 68z^2 \right) - \frac{1}{4} \left(157 - 442z + 305z^2 \right) - \frac{1}{2} \left(31 - 201z + 174z^2 \right) H_0(z) \\
 + \left(-26 + 135z - 88z^2 \right) H_1(z) + \frac{1}{2} \left(-11 + 60z - 4z^2 \right) H_{0,0}(z) - 2(7 - 48z \\
 + 48z^2) H_{0,1}(z) + \left(-23 + 72z - 56z^2 \right) H_{1,0}(z) - 2(23 - 80z + 63z^2) H_{1,1}(z) \\
 - 8(1+z)(-1+3z) H_{-1,0}(z) + \left(-17 + 34z - 52z^2 \right) H_{0,0,0}(z) - 8(3 - 6z \\
 + 10z^2) H_{0,0,1}(z) - 2(11 - 22z + 40z^2) H_{0,1,0}(z) - 6(7 - 14z + 22z^2) H_{0,1,1}(z) \\
 + 8(1 - 2z + 2z^2) H_{0,-1,0}(z) - 2(-1 + 2z + 6z^2) H_{1,0,0}(z) - 4(9 - 18z \\
 + 20z^2) H_{1,0,1}(z) - 4(7 - 14z + 16z^2) H_{1,1,0}(z) - 70(1 - 2z + 2z^2) H_{1,1,1}(z) \left. \right\} \quad (4.23)
 \end{aligned}$$

$$\Delta_{q\gamma}^{(1,1)} = 2C_A C_F \Delta_{qg}^{(1,1)} \quad (4.24)$$

$$\begin{aligned}
 \Delta_{qq}^{(1,1)} = c_q^{(2)} C_F \left\{ \zeta_2 \left(64 + 144z - 48z^2 + \left(-160 + 192z - 32z^2 + \frac{288}{1+z} \right) H_0(z) \right) \right. \\
 \left. - 32(1-z)^2 H_1(z) + \left(192 - 192z - \frac{448}{1+z} \right) H_{-1}(z) \right) - 16\zeta_3 \left(11 - 11z - \frac{26}{1+z} \right)
 \end{aligned}$$

$$\begin{aligned}
& -196+248z-52z^2+8(-16+13z)H_0(z)+128(-1+z)H_1(z) \\
& -16(5+3z^2)H_{0,0}(z)-64(1+z)H_{0,1}(z)+16(1-z)(-1+3z)H_{1,0}(z) \\
& +32(1+z)H_{-1,0}(z)+\left(16+16z-32z^2-\frac{128}{1+z}\right)H_{0,0,0}(z) \\
& +\left(64-64z-\frac{128}{1+z}\right)H_{0,0,1}(z)-\left(64-96z+32z^2-\frac{64}{1+z}\right)H_{0,1,0}(z) \\
& -\left(+64-64z-\frac{192}{1+z}\right)H_{0,-1,0}(z)-32(1-z)^2H_{1,0,0}(z)-32(1-z)^2H_{1,1,0}(z) \\
& -\left(192-192z-\frac{448}{1+z}\right)H_{-1,0,0}(z)-\left(128-128z-\frac{256}{1+z}\right)H_{-1,0,1}(z) \\
& +\left(128-128z-\frac{384}{1+z}\right)H_{-1,-1,0}(z)\}. \tag{4.25}
\end{aligned}$$

$$\begin{aligned}
\Delta_{g\bar{g}}^{(1,1)} &= C_A \left(\sum_q c_q^{(2)} \right) \left\{ \zeta_2 \left(40z+16z^2+16(1+3z+3z^2)H_0(z)-16(1+z)^2H_{-1}(z) \right) \right. \\
& +\zeta_3 \left(8-48z+32z^2 \right) -64-132z+196z^2+2(-23-64z+105z^2)H_0(z) \\
& +4(-1+z)(7+67z)H_1(z)-8(1+z)(3+4z)H_{0,0}(z)-8(1+8z-4z^2)H_{0,1}(z) \\
& +48(-1+z)(1+3z)H_{1,0}(z)+64(-1+z)(1+3z)H_{1,1}(z)+16(1+z)H_{-1,0}(z) \\
& -8(3+8z+8z^2)H_{0,0,0}(z)-16(1+2z)^2H_{0,0,1}(z)-24(1+2z)^2H_{0,1,0}(z) \\
& -32(1+2z)^2H_{0,1,1}(z)+16(1+2z+2z^2)H_{0,-1,0}(z)-16(-1+z)^2H_{1,0,0}(z) \\
& \left. +48(1+z)^2H_{-1,0,0}(z)-32(1+z)^2H_{-1,-1,0}(z) \right\}. \tag{4.26}
\end{aligned}$$

For completeness, we report the one-loop results.

$$\Delta_{q\bar{q}}^{(0,1)} = c_q^{(2)} \left\{ \delta(1-z)(-16+8\zeta_2) + 16\mathcal{D}_1 - \frac{4(1+z^2)}{(1-z)}H_0(z) + 8(1+z)H_0(z) \right\}. \tag{4.27}$$

$$\Delta_{q\gamma}^{(0,1)} = c_q^{(2)} C_A \left\{ (1-z)(1+7z) - 2(1-2z+2z^2)(H_0(z) + 2H_1(z)) \right\}. \tag{4.28}$$

4.4 The partonic coefficients for Z

$\Delta_Z^{(1,1)}$ represents the contribution to the total hadronic cross-section with a single internal Z boson. $\Delta_Z^{(1,1)}$ has the following dependency on the partonic cross-sections convoluted with PDFs

$$\begin{aligned}
\Delta_Z^{(1,1)} &= \sum_{q \in Q, \bar{Q}} f_q \otimes f_{\bar{q}} \otimes \Delta_{q\bar{q},Z}^{(1,1)} + \sum_{q \in Q, \bar{Q}} (f_q \otimes f_g + f_g \otimes f_q) \otimes \Delta_{qg,Z}^{(1,1)} \\
&+ \sum_{q \in Q, \bar{Q}} f_q \otimes f_q \otimes \Delta_{qq,Z}^{(1,1)}. \tag{4.29}
\end{aligned}$$

Below we present the partonic cross-sections. To renormalize UV divergences, only the quark wave function renormalisation has been performed in these results. The $q\bar{q}$ initiated

partonic cross-section is given by

$$\begin{aligned}
\Delta_{q\bar{q},Z}^{(1,1)} = c_q^{(4)} C_F \left\{ \delta(1-z) \left(204 - 256 \text{Li}_4\left(\frac{1}{2}\right) - \frac{32 \ln^4(2)}{3} - 172\zeta_2 + 144 \ln(2)\zeta_2 \right. \right. \\
- 128 \ln^2(2)\zeta_2 + \frac{384}{5}\zeta_2^2 - 56\zeta_3 \Big) + \mathcal{D}_1 \left(-176 + 128\zeta_2 \right) - 16 + 4z - 8\bar{z} + (-28 \\
- 68z + 80\bar{z} - 8\bar{z}^2) H_0(z) - (88 + 88z - (32 + 32z)\zeta_2) H_1(z) + 8(5 + 15z + 4z^2 \\
+ 2z^3) H_{0,0}(z) + 8(-2 + 8z + 3z^2 + z^3) H_{1,0}(z) - 8(1+z)(7+z^2) H_{-1,0}(z) \\
- (224 + 160z - 256\bar{z}) H_{0,0,0}(z) - (112 + 80z - 128\bar{z}) H_{0,1,0}(z) + (112 + 80z \\
- 128\bar{z}) H_{0,-1,0}(z) - 16(5-z) H_{1,0,0}(z) - 16(3+z) H_{1,1,0}(z) + 32(1-z) H_{1,-1,0}(z) \\
+ (192 + 64z - 256\bar{z}) H_{-1,0,0}(z) + (96 + 32z - 128\bar{z}) H_{-1,1,0}(z) + (-96 - 32z \\
+ 128\bar{z}) H_{-1,-1,0}(z) - (64 - 32z - 40z^2 - 8z^3 + \ln(2)(96 + 96z - 192\bar{z})) \zeta_2 \\
\left. + (48 + 16z - 64\bar{z}) H_{-1}(z) \zeta_2 + 16(-1 + 7\bar{z}) \zeta_3 + \frac{\delta_{q\bar{q},Z}}{z} \right\}, \tag{4.30}
\end{aligned}$$

where we used the combination of vector and axial-vector couplings $c_q^{(4)}$ defined in eq. (4.18), and where $\delta_{q\bar{q},Z}$ stems from the double-real channel $q\bar{q} \rightarrow q\bar{q}Z$, which does not produce any singularities. It is given as

$$\begin{aligned}
\delta_{q\bar{q},Z} = \frac{8(1+2z)^2}{3z^2} I_{\text{ell}}^{(0,1)} + \frac{8\tilde{z}}{3z^2} (7 + 77z + 264z^2 + 362z^3 + 136z^4) I_{\text{ell}}^{(3,0)} + \frac{8\tilde{z}}{3z} (-7 - 32z \\
+ 6z^2 + 232z^3 + 224z^4) I_{\text{ell}}^{(2,0)} + 2z\tilde{z}\hat{z}(281 - 1537z + 1829z^2 - 553z^3 - 36z^4 - 32z^5) \\
- 4z\tilde{z}^2\hat{z}^2(-91 + 803z - 2037z^2 + 890z^3 + 987z^4 - 612z^5 - 112z^6 + 64z^7) H_0(z) \\
- \frac{4}{3}\tilde{z}^2\bar{\tilde{z}}\hat{z}^2\tilde{z}(35 - 459z + 1687z^2 + 434z^3 - 10524z^4 - 248z^5 + 41084z^6 - 14160z^7 \\
- 59984z^8 + 40320z^9 + 3840z^{10}) H_{0,0}(z) + \frac{16\tilde{z}}{3} (-7 - 32z + 6z^2 + 232z^3 \\
+ 224z^4) H_{0,1}(z) + 8z\tilde{z}^2\bar{\tilde{z}}\hat{z}^2(16 - 174z + 661z^2 - 988z^3 + 395z^4 + 334z^5 - 376z^6 \\
+ 96z^7) H_{1,0}(z) - 32z\tilde{z}^2(8 + 9z - 20z^2 - 13z^3 + 15z^4 + 3z^5) H_{-1,0}(z) \\
- 32z\tilde{z} H_{\frac{1}{2},0,0}(z) - 32z\tilde{z} H_{\frac{1}{2},1,0}(z) + \frac{4\tilde{z}^3\bar{\tilde{z}}}{3} (3 + 91z - 7z^2 - 691z^3 + 264z^4 + 976z^5 \\
- 500z^6 - 388z^7 + 60z^8 + 120z^9) H_{0,0,0}(z) + \frac{16}{3} (1+2z)^2 (5 - 5z + 12z^2) \bar{\tilde{z}} H_{0,0,1}(z) \\
- \frac{8\tilde{z}^3\bar{\tilde{z}}}{3} (-4 + 9z - 7z^2 + 85z^3 - 253z^4 + 310z^5 - 144z^6 + 16z^7) H_{0,1,0}(z) \\
+ \frac{64}{3} (1-4z)(1+2z)^2 H_{0,1,1}(z) + \frac{32\tilde{z}^3}{3} (2 - 2z - 8z^2 - 12z^3 + 44z^4 - 25z^5 - 23z^6 \\
+ 9z^7 + 9z^8) H_{0,-1,0}(z) - \frac{16\tilde{z}\bar{\tilde{z}}}{3} (-1 + 5z - 6z^2 - 32z^3 + 64z^4 + 24z^5) H_{1,0,0}(z) \\
+ 32z(1+3z) H_{1,-1,0}(z) + 16z(1+z)^2 (-12 + 11z + 5z^2 + 5z^3) \bar{\tilde{z}} H_{-1,0,0}(z)
\end{aligned}$$

$$\begin{aligned}
 & -32z(1+z)^2(3-4z)\bar{z}H_{-1,1,0}(z) + 32z(1+z)^2(3-z-3z^2-3z^3)\bar{z}H_{-1,-1,0}(z) \\
 & -192\ln 2z(-1-z+2z^2+z^3)\bar{z}\zeta_2 + \left(-\frac{8}{3}\bar{z}\bar{z}\hat{z}^2\tilde{z}(-14+96z+170z^2-2141z^3\right. \\
 & + 735z^4 + 15194z^5 - 17924z^6 - 17544z^7 + 21248z^8 + 1152z^9) + 224z\bar{z}H_{\frac{1}{2}}(z) \\
 & - 8\bar{z}\bar{z}(2+z-19z^2+66z^3-36z^4-90z^5+30z^6+12z^7)H_0(z) \\
 & - 16z(11-z+6z^2)\bar{z}H_1(z) - 16z(1+z)^2(3-7z+3z^2+3z^3)\bar{z}H_{-1}(z)\Big)\zeta_2 \\
 & + \frac{16}{3}z\bar{z}^3\bar{z}(14-17z-209z^2+546z^3-241z^4-385z^5+352z^6-18z^7-36z^8)\zeta_3 \\
 & + 48t\hat{t}^4H_{-1,0,0}(t)P_2 - 8t(-1+2t)\bar{t}^4\tilde{t}^3\check{t}H_0(t)P_4 + 8t\bar{t}^4\tilde{t}^2\check{t}H_{-1}(t)P_4 \\
 & - 64t\bar{t}^5\tilde{t}^5H_{0,0,-1}(t)P_5 - 24t\bar{t}^5\tilde{t}^5H_{0,\{3,0\},0}(t)P_5 + 48t\bar{t}^5\tilde{t}^5H_{0,\{3,0\},-1}(t)P_5 \\
 & - 48t\bar{t}^5\tilde{t}^5H_{0,\{3,1\},0}(t)P_5 + 96t\bar{t}^5\tilde{t}^5H_{0,\{3,1\},-1}(t)P_5 - 16t\bar{t}^5\tilde{t}^5H_{0,-1,0}(t)P_5 \\
 & + 32t\bar{t}^5\tilde{t}^5H_{0,-1,-1}(t)P_5 - 64t\hat{t}^5\tilde{t}^5\zeta_3P_6 + 8t\hat{t}^5\tilde{t}^5H_{0,0,0}(t)P_9 + 12t\hat{t}^4\tilde{t}^4\check{t}^2H_{0,0}(t)P_{11} \\
 & + i\pi\left(16t\hat{t}^4\tilde{t}^4\zeta_2P_1 + 32t\hat{t}^4\tilde{t}^4H_{-1,0}(t)P_2 + 8t\bar{t}^3\tilde{t}^3\check{t}P_4 + 16t\bar{t}^5\tilde{t}^5H_{0,0}(t)P_7\right. \\
 & + 8t\hat{t}^4\tilde{t}^4\check{t}^2H_0(t)P_{11} - 96t\hat{t}H_{\{3,0\},0}(t) - 192t\hat{t}H_{\{3,1\},0}(t) + 256t\hat{t}H_{\{4,1\},0}(t)\Big) \\
 & - 144t\hat{t}H_{\{3,0\},0,0}(t) - 288t\hat{t}H_{\{3,1\},0,0}(t) + 384t\hat{t}H_{\{4,1\},0,0}(t) - \left(64t\hat{t}^4H_{-1}(t)P_3\right. \\
 & \left. + 8t\hat{t}^5\tilde{t}^5H_0(t)P_8 + 16t\hat{t}^4\tilde{t}^4\check{t}^2P_{10}\right)\zeta_2. \tag{4.31}
 \end{aligned}$$

The above polynomials P_i are defined as follows:

$$\begin{aligned}
 P_1 &= t^4 + 4t^3 + 10t^2 + 4t + 1. \\
 P_2 &= 3t^4 + 12t^3 + 22t^2 + 12t + 3. \\
 P_3 &= 5t^4 + 20t^3 + 34t^2 + 20t + 5. \\
 P_4 &= 8t^6 - 23t^5 + 32t^4 + 2t^3 + 32t^2 - 23t + 8. \\
 P_5 &= 3t^8 - 10t^6 + 38t^4 - 10t^2 + 3. \\
 P_6 &= 2t^{10} - 5t^8 - 4t^7 + 24t^6 + 4t^4 + 4t^3 - 2t^2 + 1. \\
 P_7 &= 11t^{10} - 35t^8 - 16t^7 + 126t^6 - 14t^4 + 16t^3 + 7t^2 + 1. \\
 P_8 &= 35t^{10} - 119t^8 - 64t^7 + 420t^6 - 140t^4 + 64t^3 + 49t^2 - 5. \\
 P_9 &= 45t^{10} - 133t^8 - 48t^7 + 490t^6 + 70t^4 + 48t^3 - 7t^2 + 15. \\
 P_{10} &= 4t^{12} + 10t^{11} + 14t^{10} + 12t^9 + 57t^8 + 198t^7 + 274t^6 + 198t^5 + 57t^4 + 12t^3 \\
 & \quad + 14t^2 + 10t + 4. \\
 P_{11} &= 5t^{12} + 10t^{11} + 16t^{10} + 4t^9 + 59t^8 + 194t^7 + 288t^6 + 194t^5 + 59t^4 + 4t^3 \\
 & \quad + 16t^2 + 10t + 5.
 \end{aligned}$$

The partonic cross-section from qg initiated channels is given by

$$\begin{aligned}
 \Delta_{qg,Z}^{(1,1)} = c_q^{(4)} \bigg\{ & -\frac{\bar{z}}{2}(25 + 11z - 105z^2 + 57z^3 + 8z^4) - (1 + 24z - 91z^2 + 92z^3 - 16z^4 - 16z^5 \\
 & + 4z^6)\bar{z}^2 H_0(z) + (16 - 50z + 58z^2 + 8z^3 - 4z^4)H_1(z) - 2\bar{z}^2(3 - 20z + 52z^2 \\
 & - 68z^3 + 36z^4)H_{\frac{1}{2},0}(z) - 2\bar{z}^2(3 - 20z + 52z^2 - 68z^3 + 36z^4)H_{\frac{1}{2},1}(z) - 2\bar{z}^2(5 - 58z \\
 & + 121z^2 - 112z^3 + 50z^4)H_{0,0}(z) - 4\bar{z}^2(2 - 13z + 23z^2 - 27z^3 + 18z^4)H_{0,1}(z) \\
 & - 2(4 - 22z + 19z^2)H_{1,0}(z) - 2(1+z)(3+5z)H_{-1,0}(z) + 8(1-2z)^2 H_{\frac{1}{2},\frac{1}{2},0}(z) \\
 & + 8(1-2z)^2 H_{\frac{1}{2},\frac{1}{2},1}(z) + 24(1-2z)^2 H_{\frac{1}{2},0,0}(z) + 24(1-2z)^2 H_{\frac{1}{2},0,1}(z) \\
 & - 6(1-4z+8z^2)H_{0,0,0}(z) - 2(1-4z+8z^2)H_{0,0,1}(z) + 4(1-4z+8z^2)H_{0,-1,0}(z) \\
 & - 24(1-2z)^2 H_{1,\frac{1}{2},0}(z) - 24(1-2z)^2 H_{1,\frac{1}{2},1}(z) - 16(5-16z+16z^2)H_{1,0,0}(z) \\
 & - 48(1-2z)^2 H_{1,0,1}(z) - 16(1-2z+2z^2)H_{1,1,0}(z) + 16(1-2z+2z^2)H_{1,-1,0}(z) \\
 & + \left(24 \ln(2)(1-2z+2z^2) + (-34+200z-490z^2+540z^3-222z^4)\bar{z}^2 \right. \\
 & + 2(1-4z+8z^2)H_0(z) - 48(1-3z+3z^2)H_1(z) \bigg) \zeta_2 + 2(19-54z+70z^2 \\
 & - 9(1-4z+8z^2)) \zeta_3 + P_{12} \left(-2w^2 \bar{w} (7H_{0,0}(w) + 4H_{0,1}(w) - 3H_{0,-i_2}(w) \right. \\
 & + 3H_{0,i_1}(w) - 4H_{0,-1}(w) - H_{1,-i_2}(w) - H_{-1,-i_2}(w) + H_{1,0}(w) + H_{1,i_1}(w) \\
 & + H_{-1,0}(w) + H_{-1,i_1}(w)) + 6w^2 \bar{w} \zeta_2 \bigg) + P_{13} \left(2w^2 \bar{w} (7H_{0,0,0}(w) + 4H_{0,0,1}(w) \right. \\
 & - 3H_{0,0,-i_2}(w) + 3H_{0,0,i_1}(w) - 4H_{0,0,-1}(w) - H_{0,1,-i_2}(w) - H_{0,-1,-i_2}(w) \\
 & + 7H_{1,0,0}(w) + 4H_{1,0,1}(w) - 3H_{1,0,-i_2}(w) + 3H_{1,0,i_1}(w) - 4H_{1,0,-1}(w) - H_{1,1,-i_2}(w) \\
 & - H_{1,-1,-i_2}(w) + 7H_{-1,0,0}(w) + 4H_{-1,0,1}(w) - 3H_{-1,0,-i_2}(w) + 3H_{-1,0,i_1}(w) \\
 & - 4H_{-1,0,-1}(w) - H_{-1,1,-i_2}(w) - H_{-1,-1,-i_2}(w) + H_{0,1,0}(w) + H_{0,1,i_1}(w) \\
 & + H_{0,-1,0}(w) + H_{0,-1,i_1}(w) + H_{1,1,0}(w) + H_{1,1,i_1}(w) + H_{1,-1,0}(w) + H_{1,-1,i_1}(w) \\
 & + H_{-1,1,0}(w) + H_{-1,1,i_1}(w) + H_{-1,-1,0}(w) + H_{-1,-1,i_1}(w)) \\
 & \left. - 6w^2 \bar{w} (H_0(w) + H_1(w) + H_{-1}(w)) \zeta_2 \right) \bigg\} \tag{4.32}
 \end{aligned}$$

where the polynomials P_{12} and P_{13} are defined as

$$P_{12} = (-1 + 6z - 4z^2 + 24z^3)/z^2 \quad \text{and} \quad P_{13} = (1 - 4z + 8z^2)/z^2. \tag{4.33}$$

The partonic cross-section from qq initiated channel, only with double real emission, is also

free of any divergences and is given by

$$\begin{aligned}
 \Delta_{qq,Z}^{(1,1)} = c_q^{(4)} C_F \Big\{ & -\frac{4}{3z^3}(-1+2z)I_{\text{ell}}^{(0,1)} + 2(1-z)(-103-172z-83z^2+4z^3)\tilde{z}^2 \\
 & -\frac{4}{3z^2}(13-28z+44z^2+16z^3)\tilde{\tilde{z}}I_{\text{ell}}^{(2,0)} - \frac{4}{3z^3}(-13-65z+52z^2+116z^3)\tilde{\tilde{z}}I_{\text{ell}}^{(3,0)} \\
 & -8\tilde{z}^3(23+56z+64z^2+27z^3+6z^4+z^5)H_0(z) + \frac{2\bar{z}\tilde{z}^2\tilde{\tilde{z}}}{3z}(-65-185z-455z^2 \\
 & -551z^3+376z^4+1444z^5+336z^6-252z^7+72z^8)H_{0,0}(z) - \frac{8}{3z}(13-28z+44z^2 \\
 & +16z^3)\tilde{\tilde{z}}H_{0,1}(z) + 8(1-z)\tilde{z}^2(8+18z+5z^2-2z^3+z^4)H_{1,0}(z) + 16\tilde{z}^2(7+17z \\
 & +17z^2+z^3-3z^4+z^5)H_{-1,0}(z) - 96(1-2z)H_{-\frac{1}{2},0,0}(z) + 96(1-2z)H_{-\frac{1}{2},-1,0}(z) \\
 & -\frac{2}{3z}\bar{z}\tilde{z}^3\tilde{\tilde{z}}(-3-82z-212z^2-122z^3+211z^4+124z^5+388z^6+272z^7)H_{0,0,0}(z) \\
 & -\frac{8}{3z}(-1+2z)(5-5z+12z^2)\bar{z}H_{0,0,1}(z) - \frac{8}{3z}\bar{z}\tilde{z}^3\tilde{\tilde{z}}(-2+6z+19z^2-83z^3 \\
 & -173z^4-47z^5+132z^6+76z^7)H_{0,1,0}(z) + \frac{32}{3z}(-1+2z)(-1+4z)H_{0,1,1}(z) \\
 & +\frac{16}{3z}\bar{z}\tilde{z}^3(2-z-2z^2+18z^3-22z^4-35z^5-8z^6)H_{0,-1,0}(z) + \frac{8}{3z}\bar{z}\tilde{z}(1+25z \\
 & -73z^2+65z^3-30z^4)H_{1,0,0}(z) - 64(1-z)^2\tilde{\tilde{z}}H_{1,-1,0}(z) + 16(21+45z-4z^2 \\
 & -44z^3)\tilde{\tilde{z}}\tilde{\tilde{z}}H_{-1,0,0}(z) + 64(1+4z+z^2-4z^3)\tilde{\tilde{z}}\tilde{\tilde{z}}H_{-1,1,0}(z) - 32(9+15z-2z^2 \\
 & -12z^3)\tilde{\tilde{z}}\tilde{\tilde{z}}H_{-1,-1,0}(z) + 192\ln(2)(-1-2z+z^2+z^3)\tilde{\tilde{z}}\tilde{\tilde{z}}\zeta_2 \\
 & +\left(\frac{8}{3z}\tilde{z}^2\tilde{\tilde{z}}(13+43z+172z^2+250z^3+82z^4-20z^5) + 48(1-2z)H_{-\frac{1}{2}}(z) \right. \\
 & -\frac{8}{z}\bar{z}\tilde{z}^3\tilde{\tilde{z}}(1+3z-3z^2-33z^3-42z^4-12z^5+10z^6+4z^7)H_0(z) \\
 & \left. -32(1-z)^2\tilde{\tilde{z}}H_1(z) - 16(5-z-6z^2+4z^3)\tilde{\tilde{z}}\tilde{\tilde{z}}H_{-1}(z)\right)\zeta_2 \\
 & \left. -\frac{16}{3}\bar{z}\tilde{z}^3\tilde{\tilde{z}}(5+22z+7z^2-50z^3-62z^4-5z^5+11z^6)\zeta_3\right\}. \tag{4.34}
 \end{aligned}$$

4.5 The partonic coefficients for W

In this section, we provide the total partonic cross-sections stemming from all the channels with Feynman diagrams where one or two internal W bosons are exchanged. Like before, the hadronic cross-section receives contributions from several partonic cross-sections convoluted

with the PDFs as:

$$\begin{aligned}
\Delta_W^{(1,1)} &= \sum_{q \in Q, \bar{Q}} f_q \otimes f_{\bar{q}} \otimes \Delta_{q\bar{q},W}^{(1,1)} + \sum_{q \in Q, \bar{Q}} f_q \otimes f_g \otimes \Delta_{qg,W}^{(1,1)} + \sum_{q \in Q, \bar{Q}} f_g \otimes f_q \otimes \Delta_{qg,W}^{(1,1)} \\
&+ \sum_{q \in Q, \bar{Q}} f_q \otimes f_q \otimes \Delta_{qq,W}^{(1,1)} \\
&+ \sum_{q \in Q, \bar{Q}} f_q \otimes f_{\bar{q}} \otimes \left((-\delta_s \Delta r^{(1,1)} + \delta g_Z^{(1,1)}) \Delta_{q\bar{q}}^{(0,0)} + 2\delta s_W^2 {}^{(1,1)} \bar{\Delta}_{q\bar{q}}^{(0,0)} \right) \\
&+ \sum_{q \in Q, \bar{Q}} f_q \otimes f_{\bar{q}} \otimes \left((-\delta_s \Delta r^{(0,1)} + \delta g_Z^{(0,1)}) \Delta_{q\bar{q}}^{(1,0)} + 2\delta s_W^2 {}^{(0,1)} \bar{\Delta}_{q\bar{q}}^{(1,0)} \right) \\
&+ \sum_{q \in Q, \bar{Q}} f_q \otimes f_g \otimes \left((-\delta_s \Delta r^{(0,1)} + \delta g_Z^{(0,1)}) \Delta_{qg}^{(1,0)} + 2\delta s_W^2 {}^{(0,1)} \bar{\Delta}_{qg}^{(1,0)} \right), \quad (4.35)
\end{aligned}$$

where $\Delta r^{(1,1)}$, $\delta g_Z^{(1,1)}$ and $\delta s_W^2 {}^{(1,1)}$ ($\Delta r^{(0,1)}$, $\delta g_Z^{(0,1)}$ and $\delta s_W^2 {}^{(0,1)}$) are finite renormalisation constants introduced in section 2.2.2 and evaluated at $\mathcal{O}(\alpha\alpha_s)$ (at $\mathcal{O}(\alpha)$). The flag δ_s is introduced to shorten the notation: its value is 1 in the G_μ input scheme and 0 in the $\alpha(0)$ scheme. $\bar{\Delta}_{ij}^{(m,n)}$ are the finite partonic cross sections, defined as:

$$\bar{\Delta}_{ij}^{(m,n)} = \frac{-Q_q C_{v,q}}{C_{v,q}^2 + C_{a,q}^2} \Delta_{ij}^{(m,n)}, \quad (\text{for } (0,0) \text{ and } (1,1)). \quad (4.36)$$

We present here the results for u -type quark only. One can easily obtain the results for d -type quarks through appropriate transformations. For example, $\Delta_{d\bar{d},W}^{(1,1)}$ can be obtained from $\Delta_{u\bar{u},W}^{(1,1)}$ through $\{u \leftrightarrow d\}$. Below we present the NNLO partonic contributions. In these results, as earlier, only the quark wave function renormalisation has been performed. The $u\bar{u}$ initiated partonic cross-section is given by

$$\begin{aligned}
\Delta_{u\bar{u},W}^{(1,1)} &= c_u^2 C_F \left\{ \delta(1-z) \left(51 - 64\text{Li}_4(1/2) - \frac{8\ln^4(2)}{3} - 43\zeta_2 + 36\ln(2)\zeta_2 - 32\ln^2(2)\zeta_2 \right. \right. \\
&+ \left. \frac{96}{5}\zeta_2^2 - 14\zeta_3 \right) + \mathcal{D}_1 \left(-44 + 32\zeta_2 \right) - (-3+z)(-2+z)\bar{z} + (11 - 23z + 27z^2 \\
&- 17z^3)\bar{z}^2 H_0(z) - 22(1+z)H_1(z) + 2(5 + 15z + 4z^2 + 2z^3)H_{0,0}(z) - 2(2 - 8z \\
&- 3z^2 - z^3)H_{1,0}(z) - 2(1+z)(7+z^2)H_{-1,0}(z) + 8(1+2z+5z^2)\bar{z}H_{0,0,0}(z) \\
&+ 4(1+2z+5z^2)\bar{z}H_{0,1,0}(z) - 4(1+2z+5z^2)\bar{z}H_{0,-1,0}(z) - 4(5-z)H_{1,0,0}(z) \\
&- 4(3+z)H_{1,1,0}(z) + 8(1-z)H_{1,-1,0}(z) - 16(1+z)^2\bar{z}H_{-1,0,0}(z) \\
&- 8(1+z)^2\bar{z}H_{-1,1,0}(z) + 8(1+z)^2\bar{z}H_{-1,-1,0}(z) + \left(2(-8+4z+5z^2+z^3) \right. \\
&+ \left. 24\ln(2)(1+z^2)\bar{z} + 8(1+z)H_1(z) - 4(1+z)^2\bar{z}H_{-1}(z) \right) \zeta_2 + 4(6+z)\bar{z}\zeta_3 \left. \right\} \\
&+ c_u(c_u - c_d)C_F \left\{ \delta(1-z) \left(-20 + 64\text{Li}_4(1/2) + \frac{8\ln^4(2)}{3} + \frac{467}{6}\zeta_2 - 36\ln(2)\zeta_2 \right. \right.
\end{aligned}$$

$$\begin{aligned}
 & + 32 \ln^2(2)\zeta_2 - \frac{278}{5}\zeta_2^2 + \frac{46}{3}\zeta_3 + \frac{67}{2}\sqrt{3}G_I(r_2) - 20\sqrt{3}\zeta_2 G_I(r_2) + 7\sqrt{3}G_I(0, r_2) \\
 & - 4G_I(r_2)G_I(0, r_2) + 24G_I(0, r_2)^2 \Big) + \mathcal{D}_1 \left(16 - 64\zeta_2 - 40\sqrt{3}G_I(r_2) \right) + 20 - 16z \\
 & - 4(-2 + z + 2z^2)\bar{z}H_0(z) + 8(1 + z)H_1(z) - 2(4 + 16z + 9z^2 + 3z^3)H_{0,0}(z) \\
 & - 4(2 - z)zH_{1,0}(z) - 2(1 + z)(-9 + 4z + z^2)H_{\{6,0\},0}(z) - 2(1 + z)(3 - 8z \\
 & - 2z^2)H_{\{6,1\},0}(z) + 2(1 + z)(7 + z^2)H_{-1,0}(z) - 4(2 + 3z + 11z^2)\bar{z}H_{0,0,0}(z) \\
 & - 4(1 + 3z + 4z^2)\bar{z}H_{0,1,0}(z) + 4zH_{0,\{6,0\},0}(z) - 8zH_{0,\{6,1\},0}(z) \\
 & + 4(1 + 2z + 5z^2)\bar{z}H_{0,-1,0}(z) + 28H_{1,0,0}(z) + 4H_{1,1,0}(z) + 4(2 + z)H_{1,\{6,0\},0}(z) \\
 & - 8(2 + z)H_{1,\{6,1\},0}(z) - 8(1 - z)H_{1,-1,0}(z) + 16(1 + z)^2\bar{z}H_{-1,0,0}(z) \\
 & + 8(1 + z)^2\bar{z}H_{-1,1,0}(z) - 8(1 + z)^2\bar{z}H_{-1,-1,0}(z) + \left(-24 \ln(2)(1 + z^2)\bar{z} \right. \\
 & + \frac{1}{3}(63 - 13z - 70z^2 - 14z^3) + \frac{8}{3}(1 + z)(1 + 2z)\bar{z}H_0(z) - \frac{8}{3}(7 + 8z)H_1(z) \\
 & \left. + 4(1 + z)^2\bar{z}H_{-1}(z) \right) \zeta_2 - \frac{4}{3}(24 + 11z + 22z^2)\bar{z}\zeta_3 + \left(2(1 - z)(-3 + z)\sqrt{3} \right. \\
 & + 20z^2\bar{z}\sqrt{3}H_0(z) - 20(1 + z)\sqrt{3}H_1(z) - 2(1 + z)(1 + 4z + z^2)\sqrt{3}H_{\{6,0\}}(z) \\
 & + 10(1 + z)\sqrt{3}H_{\{6,1\}}(z) + 4z\sqrt{3}H_{0,\{6,0\}}(z) + 4(2 + z)\sqrt{3}H_{1,\{6,0\}}(z) \\
 & \left. - 16G_I(0, r_2) \right) G_I(r_2) - 10(1 + z)\sqrt{3}G_I(0, r_2) \\
 & + 12\hat{\rho}(1 - \rho)(1 + \rho) \left(H_{0,0}(\rho) + H_{0,\{6,0\}}(\rho) - 2H_{0,\{6,1\}}(\rho) \right) \\
 & + 12\bar{\rho}^2\hat{\rho}(1 - \rho + 6\rho^2 - \rho^3 + \rho^4) \left(H_{0,0,0}(\rho) + H_{0,0,\{6,0\}}(\rho) - 2H_{0,0,\{6,1\}}(\rho) \right) \\
 & \left. - \left(4\hat{\rho}(1 - \rho)(1 + \rho) + 4\bar{\rho}^2\hat{\rho}(1 - \rho + 6\rho^2 - \rho^3 + \rho^4)H_0(\rho) \right) \zeta_2 \right\} \\
 & + \delta_{u\bar{u},W}^{(1)} + \delta_{u\bar{u},W}^{(2)}, \tag{4.37}
 \end{aligned}$$

where c_q , with $q \in (u, d)$, was defined in eq. (4.19) and where $\delta_{u\bar{u},W}^{(1)}$ and $\delta_{u\bar{u},W}^{(2)}$ denote the contributions from the double-real channel $u\bar{u} \rightarrow d\bar{d}Z$ with one and two internal W boson, respectively. They are given in the following.

$$\begin{aligned}
 \delta_{u\bar{u},W}^{(1)} = & c_u^2 C_F \left\{ (44 - 65z + 29z^2)\bar{z} + (47 - 61z + 26z^2)\bar{z}^2 H_0(z) + 6(7 - 3z - z^2 \right. \\
 & + z^3)\bar{z}^2 H_{0,0}(z) - 2(-7 + 7z - 7z^2 + 3z^3)\bar{z}^2 H_{1,0}(z) - 4(1 + z)(7 - 8z \\
 & + 3z^2)\bar{z}^2 H_{-1,0}(z) + 24\bar{z}^3(1 - z + 3z^2 - 3z^3 + z^4)H_{0,0,0}(z) + 8\bar{z}^3(1 - z + 3z^2 \\
 & - 3z^3 + z^4)H_{0,1,0}(z) - 16\bar{z}^3(1 - z + 3z^2 - 3z^3 + z^4)H_{0,-1,0}(z) - 12z\zeta_2 \\
 & \left. - 8\bar{z}^3(1 - z + 3z^2 - 3z^3 + z^4)\zeta_3 \right\} + c_d^2 C_F \left\{ \frac{1}{2}(1 - z)(-21 + 27z + 8z^2) \right. \\
 & - z(-14 + 3z + 4z^2)H_0(z) + 2(5 + 28z + 35z^2 + 10z^3)H_{0,0}(z) - 4(4 + 18z + 21z^2 \\
 & + 6z^3)H_{-1,0}(z) + 4(3 + 20z + 30z^2 + 20z^3 + 5z^4)H_{0,0,0}(z) - 8(2 + 12z + 18z^2 \\
 & \left. + 12z^3 + 3z^4)H_{0,-1,0}(z) - 20(1 + z)^4 H_{-1,0,0}(z) + 24(1 + z)^4 H_{-1,-1,0}(z) \right\}
 \end{aligned}$$

$$\begin{aligned}
 & + \left(-2(4+18z+21z^2+6z^3) - 4(2+12z+18z^2+12z^3+3z^4)H_0(z) \right. \\
 & \left. + 12(1+z)^4H_{-1}(z) \right) \zeta_2 - 12(1+8z+12z^2+8z^3+2z^4)\zeta_3 \Big\} \\
 & + c_u c_d C_F \left\{ \frac{2}{3z^3}(1+2z)^2 I_{\text{ell}}^{(0,1)} + \frac{2}{3z^3} \tilde{z} (7+77z+264z^2+362z^3+136z^4) I_{\text{ell}}^{(3,0)} \right. \\
 & + \frac{2}{3z^2} \tilde{z} (-7-32z+6z^2+232z^3+224z^4) I_{\text{ell}}^{(2,0)} + 6(1-2z)(1+z)\bar{z}H_0(z) \\
 & - 4(-7+10z) - \frac{1}{3z} \bar{z} \tilde{z} (35+163z+12z^2-392z^3+734z^4+1140z^5) H_{0,0}(z) \\
 & + \frac{4}{3z} \tilde{z} (-7-32z+6z^2+232z^3+224z^4) H_{0,1}(z) - 2(5+3z^2) H_{1,0}(z) \\
 & - 4(8+28z+21z^2) H_{-1,0}(z) - \frac{\bar{z}}{3z} (-3-25z-108z^2-48z^3+16z^4) H_{0,0,0}(z) \\
 & + \frac{4}{3z} (1+2z)^2 (5-5z+12z^2) \bar{z} H_{0,0,1}(z) + \frac{4}{3z} \bar{z} (2-z-9z^2-35z^3+4z^4) H_{0,1,0}(z) \\
 & - \frac{16}{3z} (1+2z)^2 (-1+4z) H_{0,1,1}(z) + \frac{8}{3z} \bar{z} (2+11z+24z^2+13z^3+4z^4) H_{0,-1,0}(z) \\
 & + \frac{4}{3z} \bar{z} (1+3z^2+38z^3+12z^4) H_{1,0,0}(z) + 8(1+3z) H_{1,-1,0}(z) + 16(1+z)^2 (-3 \\
 & + 4z) \bar{z} H_{-1,0,0}(z) + 8(1+z)^2 (-3+4z) \bar{z} H_{-1,1,0}(z) - 8(1+z)^2 (-3+4z) \bar{z} H_{-1,-1,0}(z) \\
 & - 48 \ln(2) (-1-z+2z^2+z^3) \bar{z} \zeta_2 + \left(-\frac{2}{3z} \tilde{z} (-14-25z+174z^2+704z^3+592z^4) \right. \\
 & \left. - \frac{4}{z} \bar{z} (1+z-9z^2+14z^3+24z^4) H_0(z) + 4(1+3z) H_1(z) \right. \\
 & \left. + 4(1+z)^2 (-3+4z) \bar{z} H_{-1}(z) \right) \zeta_2 - \frac{4}{3} (-17-72z+63z^2+113z^3) \bar{z} \zeta_3 \Big\}. \quad (4.38)
 \end{aligned}$$

$$\begin{aligned}
 \delta_{u\bar{u},W}^{(2)} = & c_u (c_u - c_d) C_F \left\{ -\frac{2}{3} (35-11z+30z\sqrt{3}G_I(0,r_2)) + \frac{2}{3} (-33+7z+2z^2) \bar{z} H_0(z) \right. \\
 & - \frac{2}{3} (6+30z+60z^2+5z^3) H_{0,0}(z) - \frac{2}{3} (2-3z+12z^2+z^3) H_{1,0}(z) + 2(-4+27z \\
 & + 12z^2+z^3) H_{\{3,0\},0}(z) + 2(-8+9z+24z^2+2z^3) H_{\{3,1\},0}(z) - \frac{4}{3} (1+z) (-14 \\
 & + 11z+z^2) H_{-1,0}(z) + 4(1+2z)(1+5z) \bar{z} H_{0,0,0}(z) + 4z(2+z) \bar{z} H_{0,1,0}(z) \\
 & - 6(1+z+7z^2) \bar{z} H_{0,\{3,0\},0}(z) - 12(1+z+7z^2) \bar{z} H_{0,\{3,1\},0}(z) \\
 & + 8(1-z+6z^2) \bar{z} H_{0,-1,0}(z) + \frac{2}{3} (4+15z) \zeta_2 + \frac{4}{3} (7+z+28z^2) \bar{z} \zeta_3 \\
 & - 12\hat{\rho}(1-\rho)(1+\rho) (H_{0,0}(\rho) + H_{0,\{6,0\}}(\rho) - 2H_{0,\{6,1\}}(\rho)) \\
 & - 12\bar{\rho}^2 \hat{\rho}(1-\rho+6\rho^2-\rho^3+\rho^4) (H_{0,0,0}(\rho) + H_{0,0,\{6,0\}}(\rho) - 2H_{0,0,\{6,1\}}(\rho)) \\
 & \left. + (4\hat{\rho}(1-\rho)(1+\rho) + 4\bar{\rho}^2 \hat{\rho}(1-\rho+6\rho^2-\rho^3+\rho^4) H_0(\rho)) \zeta_2 \right\} \\
 & + c_d (c_u - c_d) C_F \left\{ 2(-7+7z+10\sqrt{3}G_I(0,r_2) + 12z\sqrt{3}G_I(0,r_2)) - 2(6+z)H_0(z) \right. \\
 & \left. + 2(-1+14z+10z^2)H_{0,0}(z) - 6(9+16z+5z^2)H_{\{3,0\},0}(z) - 6(3+14z \right.
 \end{aligned}$$

$$\begin{aligned}
 & +10z^2)H_{\{3,1\},0}(z)+4(5+14z+10z^2)H_{-1,0}(z)+4(1+11z+9z^2)H_{0,0,0}(z) \\
 & -6(1+3z+3z^2)H_{0,\{3,0\},0}(z)-12(1+3z+3z^2)H_{0,\{3,1\},0}(z)-8(-1+z)H_{0,-1,0}(z) \\
 & -48(1+z)^2H_{-1,0,0}(z)+36(1+z)^2H_{-1,\{3,0\},0}(z)+72(1+z)^2H_{-1,\{3,1\},0}(z) \\
 & -24(1+z)^2H_{-1,-1,0}(z)+\left(4-4z(4+3z)H_0(z)+12(1+z)^2H_{-1}(z)\right)\zeta_2 \\
 & +\frac{20}{3}(5+3z)\zeta_3\left. \right\}. \tag{4.39}
 \end{aligned}$$

We note that once we combine eq. (4.39) with eq. (4.37), the total ρ dependence vanishes.

The partonic cross-section from ug initiated channels is given by

$$\begin{aligned}
 \Delta_{ug,W}^{(1,1)} = c_u^2 \left\{ & -\frac{\bar{z}}{8}(1+31z-73z^2+29z^3+8z^4)-\frac{\bar{z}^2}{4}(-1+24z-81z^2+78z^3-10z^4) \right. \\
 & -16z^5+4z^6)H_0(z)+\frac{1}{2}(5-20z+22z^2+4z^3-2z^4)H_1(z)+\frac{\bar{z}^2}{2}(1-21z+38z^2 \\
 & -33z^3+19z^4)H_{0,0}(z)+\frac{1}{2}P_{15}\bar{z}^2H_{0,1}(z)+\frac{1}{2}(1+8z-10z^2)H_{1,0}(z)+\frac{\bar{z}^2}{2}(7-39z \\
 & +61z^2-45z^3+19z^4)H_{\{6,0\},0}(z)+\frac{1}{2}P_{15}\bar{z}^2H_{\{6,0\},1}(z)-\frac{\bar{z}^2}{2}(-1-30z+71z^2 \\
 & -72z^3+38z^4)H_{\{6,1\},0}(z)-P_{15}\bar{z}^2H_{\{6,1\},1}(z)+3P_{14}H_{0,0,0}(z)+P_{14}H_{0,0,1}(z) \\
 & +2P_{14}H_{0,\{6,0\},0}(z)+P_{14}H_{0,\{6,0\},1}(z)-4P_{14}H_{0,\{6,1\},0}(z)-2P_{14}H_{0,\{6,1\},1}(z) \\
 & +(7-18z+30z^2)H_{1,0,0}(z)+2P_{14}H_{1,0,1}(z)-3(1-2z+2z^2)H_{1,1,0}(z) \\
 & +3(2-5z+8z^2)H_{1,\{6,0\},0}(z)+2P_{14}H_{1,\{6,0\},1}(z)-6(2-5z+8z^2)H_{1,\{6,1\},0}(z) \\
 & -4P_{14}H_{1,\{6,1\},1}(z)+\left(\frac{\bar{z}^2}{12}(45-214z+381z^2-260z^3+38z^4)+\frac{2}{3}P_{14}H_0(z) \right. \\
 & \left. +\frac{1}{3}(13-21z+6z^2)H_1(z)\right)\zeta_2+(-1+3z-6z^2)\zeta_3+\left(-\frac{1}{4}(-4+32z-61z^2 \right. \\
 & \left. +35z^3)\bar{z}\sqrt{3}+z(-2+5z)\sqrt{3}H_0(z)+5(1-2z+2z^2)\sqrt{3}H_1(z)+\frac{\bar{z}^2}{2}(-1-z \right. \\
 & \left. +11z^2-11z^3+z^4)\sqrt{3}H_{\{6,0\}}(z)-\frac{1}{2}(-5+6z)\sqrt{3}H_{\{6,1\}}(z)+(2-3z)\sqrt{3}H_{1,\{6,0\}}(z) \right. \\
 & \left. +2(-2+3z)G_I(0,r_2)\right)G_I(r_2)+\frac{1}{2}(-5+6z)\sqrt{3}G_I(0,r_2)\left. \right\} \\
 & +c_uc_d\left\{\frac{1}{2}(-1+z)(6+7z)-\frac{1}{2}(1+z-4z^2+3z^3)\bar{z}H_0(z)+\frac{1}{2}(3-5z+7z^2)H_1(z) \right. \\
 & +\frac{\bar{z}^2}{2}(-3+20z-52z^2+68z^3-36z^4)H_{\frac{1}{2},0}(z)+\frac{\bar{z}^2}{2}(-3+20z-52z^2+68z^3 \\
 & -36z^4)H_{\frac{1}{2},1}(z)+\frac{\bar{z}^2}{2}(-6+79z-159z^2+145z^3-69z^4)H_{0,0}(z)+\frac{\bar{z}^2}{2}(-3+29z \\
 & -54z^2+65z^3-45z^4)H_{0,1}(z)-\frac{1}{2}(1-z)(5-9z)H_{1,0}(z)+\frac{\bar{z}^2}{2}(-7+39z-61z^2 \\
 & \left. +45z^3-19z^4)H_{\{6,0\},0}(z)+\frac{\bar{z}^2}{2}(1+3z-8z^2+11z^3-9z^4)H_{\{6,0\},1}(z) \right.
 \end{aligned}$$

$$\begin{aligned}
 & + \frac{\bar{z}^2}{2}(-1-30z+71z^2-72z^3+38z^4)H_{\{6,1\},0}(z) + P_{15}\bar{z}^2H_{\{6,1\},1}(z) \\
 & - \frac{1}{2}(1+z)(3+5z)H_{-1,0}(z) + 2(1-2z)^2H_{\frac{1}{2},\frac{1}{2},0}(z) + 2(1-2z)^2H_{\frac{1}{2},\frac{1}{2},1}(z) \\
 & + 6(1-2z)^2H_{\frac{1}{2},0,0}(z) + 6(1-2z)^2H_{\frac{1}{2},0,1}(z) - \frac{3}{2}(3-10z+20z^2)H_{0,0,0}(z) \\
 & + \frac{1}{2}(-3+10z-20z^2)H_{0,0,1}(z) - 2(1-3z+6z^2)H_{0,\{6,0\},0}(z) \\
 & + (-1+3z-6z^2)H_{0,\{6,0\},1}(z) + 4P_{14}H_{0,\{6,1\},0}(z) + 2(1-3z+6z^2)H_{0,\{6,1\},1}(z) \\
 & + P_{13}z^2H_{0,-1,0}(z) - 6(1-2z)^2H_{1,\frac{1}{2},0}(z) - 6(1-2z)^2H_{1,\frac{1}{2},1}(z) + (-27+82z \\
 & - 94z^2)H_{1,0,0}(z) - 2(7-27z+30z^2)H_{1,0,1}(z) + (-1+2z-2z^2)H_{1,1,0}(z) \\
 & - 3(2-5z+8z^2)H_{1,\{6,0\},0}(z) - 2(1-3z+6z^2)H_{1,\{6,0\},1}(z) + 6(2-5z \\
 & + 8z^2)H_{1,\{6,1\},0}(z) + 4P_{14}H_{1,\{6,1\},1}(z) + 4(1-2z+2z^2)H_{1,-1,0}(z) + 6\ln(2)(1 \\
 & - 2z+2z^2)\zeta_2 + \left(\frac{\bar{z}^2}{12}(-147+814z-1851z^2+1880z^3-704z^4) - \frac{1}{6}H_0(z) \right. \\
 & \left. + \frac{1}{3}(-49+129z-114z^2)H_1(z)\right)\zeta_2 + (6-12z+5z^2)\zeta_3 + \left(-\frac{1}{4}(4-32z+61z^2 \right. \\
 & - 35z^3)\bar{z}\sqrt{3} + (2-5z)z\sqrt{3}H_0(z) - 5(1-2z+2z^2)\sqrt{3}H_1(z) + \frac{\bar{z}^2}{2}(1+z-11z^2 \\
 & + 11z^3-z^4)\sqrt{3}H_{\{6,0\}}(z) + \frac{1}{2}(-5+6z)\sqrt{3}H_{\{6,1\}}(z) + (-2+3z)\sqrt{3}H_{1,\{6,0\}}(z) \\
 & \left. - 2(-2+3z)G_I(0,r_2)\right)G_I(r_2) + \frac{1}{2}(5-6z)\sqrt{3}G_I(0,r_2) + P_{12}\left(-\frac{w^2\tilde{w}}{2}(7H_{0,0}(w) \right. \\
 & + 4H_{0,1}(w) + 3H_{0,i_1}(w) - 3H_{0,-i_2}(w) - 4H_{0,-1}(w) - H_{1,-i_2}(w) - H_{-1,-i_2}(w) \\
 & + H_{1,0}(w) + H_{1,i_1}(w) + H_{-1,0}(w) + H_{-1,i_1}(w)) + \frac{3}{2}w^2\tilde{w}\zeta_2) + P_{13}\left(\frac{w^2\bar{w}}{2}(7H_{0,0,0}(w) \right. \\
 & + 4H_{0,0,1}(w) + 3H_{0,0,i_1}(w) - 3H_{0,0,-i_2}(w) - 4H_{0,0,-1}(w) - H_{0,1,-i_2}(w) \\
 & - H_{0,-1,-i_2}(w) + 7H_{1,0,0}(w) + 4H_{1,0,1}(w) + 3H_{1,0,i_1}(w) - 3H_{1,0,-i_2}(w) \\
 & - 4H_{1,0,-1}(w) - H_{1,1,-i_2}(w) - H_{1,-1,-i_2}(w) + 7H_{-1,0,0}(w) + 4H_{-1,0,1}(w) \\
 & + 3H_{-1,0,i_1}(w) - 3H_{-1,0,-i_2}(w) - 4H_{-1,0,-1}(w) - H_{-1,1,-i_2}(w) - H_{-1,-1,-i_2}(w) \\
 & + H_{0,1,0}(w) + H_{0,1,i_1}(w) + H_{0,-1,0}(w) + H_{0,-1,i_1}(w) + H_{1,1,0}(w) + H_{1,1,i_1}(w) \\
 & + H_{1,-1,0}(w) + H_{1,-1,i_1}(w) + H_{-1,1,0}(w) + H_{-1,1,i_1}(w) + H_{-1,-1,0}(w) \\
 & \left. \left. + H_{-1,-1,i_1}(w)\right) - \frac{3}{2}w^2\bar{w}(H_0(w) + H_1(w) + H_{-1}(w))\zeta_2\right)\}. \tag{4.40}
 \end{aligned}$$

P_{12} and P_{13} are given in eq. (4.33) and new polynomials are defined as

$$P_{14} = (1-3z+6z^2) \quad \text{and} \quad P_{15} = (-1-3z+8z^2-11z^3+9z^4). \tag{4.41}$$

The partonic cross-section from ud initiated channel, contributing to the double-real

corrections, is also free of any divergences and is given by

$$\begin{aligned}
\Delta_{ud,W}^{(1,1)} = & (c_u^2 + c_d^2) C_F \left\{ -\frac{1}{6z^3} (-1+2z) I_{\text{ell}}^{(0,1)} - \frac{1}{6z^2} (13-28z+44z^2+16z^3) \tilde{z} I_{\text{ell}}^{(2,0)} \right. \\
& - \frac{1}{6z^3} (-13-65z+52z^2+116z^3) \tilde{z} I_{\text{ell}}^{(3,0)} - \frac{1}{4} (1-z) (123+200z+95z^2) \tilde{z}^2 \\
& - \tilde{z}^3 (27+63z+76z^2+37z^3+6z^4) H_0(z) + \frac{1}{12z} \bar{z} \tilde{z}^2 \tilde{z} (-65-245z-287z^2 \\
& + 325z^3+544z^4+376z^5+72z^6) H_{0,0}(z) - \frac{1}{3z} (13-28z+44z^2+16z^3) \tilde{z} H_{0,1}(z) \\
& + (1-z) (-3+z^2) \tilde{z}^2 H_{1,0}(z) + 2(3+z) \tilde{z}^2 H_{-1,0}(z) - \frac{1}{12z} \bar{z} \tilde{z}^3 (-3+44z-204z^2 \\
& - 2z^3+167z^4+150z^5+40z^6) H_{0,0,0}(z) - \frac{1}{3z} (-1+2z) (5-5z+12z^2) \bar{z} H_{0,0,1}(z) \\
& - \frac{\bar{z} \tilde{z}^3}{3z} (-2+22z-z^2-33z^3-35z^4+11z^5+14z^6) H_{0,1,0}(z) + \frac{4}{3z} (-1+2z) (-1 \\
& + 4z) H_{0,1,1}(z) - \frac{2}{3z} \bar{z} \tilde{z}^3 (-2-5z+20z^2+18z^3+10z^4+5z^5+2z^6) H_{0,-1,0}(z) \\
& - \frac{1}{3z} (-1+2z) (1+2z+3z^2) \bar{z} H_{1,0,0}(z) + \left(\frac{1}{3z} \tilde{z}^2 \tilde{z} (13-2z+13z^2+103z^3+79z^4 \right. \\
& \left. + 10z^5) + \frac{\bar{z} \tilde{z}^3}{z} (-1-3z-z^2-5z^3+8z^4+18z^5+8z^6) H_0(z) \right) \zeta_2 \\
& \left. + \frac{2}{3} \bar{z} \tilde{z}^3 (-8-18z-19z^2+19z^3+36z^4+14z^5) \zeta_3 \right\} \\
& + c_u c_d C_F \left\{ 2(1-z) (5+2z+z^2) \tilde{z} - 2\tilde{z}^2 (-4-3z-9z^2-z^3+z^4) H_0(z) \right. \\
& - 2\tilde{z} (-5+24z+20z^2-12z^3+3z^4) H_{0,0}(z) + 2(1-z) (11-4z+z^2) H_{1,0}(z) \\
& + 4\tilde{z} (4+12z+5z^2-4z^3+z^4) H_{-1,0}(z) - 24(1-2z) H_{-\frac{1}{2},0,0}(z) \\
& + 24(1-2z) H_{-\frac{1}{2},-1,0}(z) + 4(5-z-6z^2+8z^3) \tilde{z} \tilde{z} H_{0,0,0}(z) + 8(1+4z^2) \tilde{z} H_{0,1,0}(z) \\
& + 8(-1+4z+z^2) \tilde{z} H_{0,-1,0}(z) + 16(1-z)^2 \tilde{z} H_{1,0,0}(z) - 16(1-z)^2 \tilde{z} H_{1,-1,0}(z) \\
& - 4(-21-45z+4z^2+44z^3) \tilde{z} \tilde{z} H_{-1,0,0}(z) - 16(-1-4z-z^2+4z^3) \tilde{z} \tilde{z} H_{-1,1,0}(z) \\
& + 8(-9-15z+2z^2+12z^3) \tilde{z} \tilde{z} H_{-1,-1,0}(z) + 48 \ln(2) (-1-2z+z^2+z^3) \tilde{z} \tilde{z} \zeta_2 \\
& + \left(-2(-15-8z+5z^2) \tilde{z} + 12(1-2z) H_{-\frac{1}{2}}(z) + 4(1+4z+17z^2+10z^3) \tilde{z} \tilde{z} H_0(z) \right. \\
& \left. - 8(1-z)^2 \tilde{z} H_1(z) - 4(5-z-6z^2+4z^3) \tilde{z} \tilde{z} H_{-1}(z) \right) \zeta_2 \\
& \left. + 4(1+3z+14z^2+13z^3) \tilde{z} \tilde{z} \zeta_3 \right\} + \delta_{ud,W}. \tag{4.42}
\end{aligned}$$

$$\begin{aligned}
\delta_{ud,W} = & (c_u - c_d)^2 C_F \left\{ \frac{1}{3} (1-z) (53+44z+3z^2) \tilde{z} \right. \\
& - \frac{\tilde{z}^2}{3} (-30-77z-85z^2-11z^3+3z^4) H_0(z) \\
& + \frac{1}{3} (15+27z-90z^2+11z^3) H_{0,0}(z) - \frac{1}{3} (1-z) (-2-11z+z^2) H_{1,0}(z) \\
& \left. + (-29+42z+27z^2-4z^3) H_{\{3,0\},0}(z) + (-13-6z+54z^2-8z^3) H_{\{3,1\},0}(z) \right\}
\end{aligned}$$

$$\begin{aligned}
 & + \frac{2}{3}(13 - 42z^2 + 7z^3)H_{-1,0}(z) + 6(1 - 2z)(1 - z)\tilde{z}H_{0,0,0}(z) + 2(1 - z \\
 & + 4z^2)\tilde{z}H_{0,1,0}(z) - 6(1 - 2z)\tilde{z}H_{0,\{3,0\},0}(z) - 12(1 - 2z)\tilde{z}H_{0,\{3,1\},0}(z) - 4(-2 + 2z \\
 & + z^2)\tilde{z}H_{0,-1,0}(z) + 8(-2 - z + 4z^2)\tilde{z}H_{-1,0,0}(z) - 6(-2 - z + 4z^2)\tilde{z}H_{-1,\{3,0\},0}(z) \\
 & - 12(-2 - z + 4z^2)\tilde{z}H_{-1,\{3,1\},0}(z) + 4(-2 - z + 4z^2)\tilde{z}H_{-1,-1,0}(z) + \left(\frac{1}{3}(2 + 3z) \right. \\
 & \left. + 2\tilde{z}\left(3z^2 + \frac{1}{\tilde{z}}\right)H_0(z) - 2(-2 - z + 4z^2)\tilde{z}H_{-1}(z)\right)\zeta_2 - \frac{2}{3}(-24 - 16z + 17z^2)\tilde{z}\zeta_3 \\
 & \left. + 10(1 - 2z)\sqrt{3}G_I(0, r_2)\right\}. \tag{4.43}
 \end{aligned}$$

The contribution $\delta_{ud,W}$ in eq. (4.42) stems solely from the non-abelian WWZ vertex. The partonic cross-section from $u\bar{d}$ initiated channel is also only with double real emission and given by

$$\begin{aligned}
 \Delta_{u\bar{d},W}^{(1,1)} = & (c_u^2 + c_d^2)C_F \left\{ -(-39 + 323z - 682z^2 + 74z^3)\hat{z}^2 - \bar{z}\hat{z}^2(-26 + 187z - 265z^2 \right. \\
 & - 296z^3 + 76z^4)H_0(z) + (11 - 78z + 129z^2 + 46z^3)\hat{z}^2H_{0,0}(z) + (11 - 78z + 129z^2 \\
 & + 46z^3)\hat{z}^2H_{1,0}(z) + 3(1 + 3z)\bar{z}H_{0,0,0}(z) + 3(1 + 3z)\bar{z}H_{0,1,0}(z) + \left((11 - 78z + 129z^2 \right. \\
 & \left. + 46z^3)\hat{z}^2 + 3(1 + 3z)\bar{z}H_0(z)\right)\zeta_2 + 6(1 + 3z)\bar{z}\zeta_3 + \frac{1}{z}\left(-\frac{1}{2}t(-1 + 2t)\bar{t}^4\bar{t}^3H_0(t)P_{16} \right. \\
 & \left. + \frac{1}{2}\bar{t}^4\bar{t}^2H_{-1}(t)P_{16} - 2\bar{t}^4\bar{t}^4H_{0,-1}(t)P_{17} - 2\bar{t}^4\bar{t}^4H_{-1,0}(t)P_{17} + 4\bar{t}^4\bar{t}^4H_{-1,-1}(t)P_{17} \right. \\
 & \left. + \bar{t}^4\bar{t}^4H_{0,0}(t)P_{19} - 8\bar{t}^5\bar{t}^5H_{0,0,-1}(t)P_{20} - 3\bar{t}^5\bar{t}^5H_{0,\{3,0\},0}(t)P_{20} \right. \\
 & \left. + 6\bar{t}^5\bar{t}^5H_{0,\{3,0\},-1}(t)P_{20} - 6\bar{t}^5\bar{t}^5H_{0,\{3,1\},0}(t)P_{20} + 12\bar{t}^5\bar{t}^5H_{0,\{3,1\},-1}(t)P_{20} \right. \\
 & \left. - 2\bar{t}^5\bar{t}^5H_{0,-1,0}(t)P_{20} + 4\bar{t}^5\bar{t}^5H_{0,-1,-1}(t)P_{20} - 2\bar{t}^5\bar{t}^5\zeta_3P_{21} + \bar{t}^5\bar{t}^5H_{0,0,0}(t)P_{23} \right. \\
 & \left. + \frac{1}{2}t(1 + t + t^2)\bar{t}^4\bar{t}^4P_{16} + i\pi\left(\frac{1}{2}\bar{t}^3\bar{t}^3P_{16} + 2\bar{t}^4\bar{t}^4H_0(t)P_{18} + 2\bar{t}^5\bar{t}^5H_{0,0}(t)P_{21} \right. \right. \\
 & \left. \left. + 4t(1 + t^2)\bar{t}^4H_{-1,0}(t) + 2t(1 + t^2)\bar{t}^4\zeta_2\right) + 6t(1 + t^2)\bar{t}^4H_{-1,0,0}(t) + (-4\bar{t}^4\bar{t}^4P_{18} \right. \\
 & \left. - \bar{t}^5\bar{t}^5H_0(t)P_{22} - 8t(1 + t^2)\bar{t}^4H_{-1}(t)\zeta_2\right\} \\
 & + c_u c_d C_F \left\{ -(15 - 127z + 236z^2 + 164z^3)\hat{z}^2 - 2\bar{z}\hat{z}^2(7 - 46z + 42z^2 + 104z^3 \right. \\
 & \left. + 28z^4)H_0(z) + 2\bar{z}\bar{z}\hat{z}^2(-2 + 12z - 12z^2 + 31z^3 - 256z^4 + 380z^5)H_{0,0}(z) \right. \\
 & \left. + 2\bar{z}\bar{z}\hat{z}^2(1 - 9z + z^2 + 132z^3 - 188z^4)H_{1,0}(z) + 12(1 + z)^2\bar{z}H_{-1,0}(z) + 16\bar{z}\bar{z}H_{0,0,0}(z) \right. \\
 & \left. + 16\bar{z}\bar{z}H_{0,0,1}(z) - 4(-2 + z + 3z^2 + 2z^3)\bar{z}\bar{z}H_{0,1,0}(z) + 8(1 + z)^2\bar{z}H_{0,-1,0}(z) \right. \\
 & \left. + 20\bar{z}\bar{z}H_{1,0,0}(z) + 16\bar{z}\bar{z}H_{1,0,1}(z) + 8\bar{z}\bar{z}H_{1,1,0}(z) + 20(1 + z)^2\bar{z}H_{-1,0,0}(z) \right. \\
 & \left. - 24(1 + z)^2\bar{z}H_{-1,-1,0}(z) + \left(2\bar{z}\bar{z}\hat{z}^2(4 - 34z + 49z^2 + 197z^3 - 416z^4 + 92z^5) \right. \right. \\
 & \left. \left. - 4(1 - 3z + 6z^2 + 4z^3)\bar{z}\bar{z}H_0(z) - 8\bar{z}\bar{z}H_1(z) - 12(1 + z)^2\bar{z}H_{-1}(z)\right)\zeta_2 - 4(-1 - z \right. \\
 & \left. + 6z^2 + 4z^3)\bar{z}\bar{z}\zeta_3 + \frac{1}{z}\left(4\bar{t}\bar{t}^4H_{1,0}(z)P_{25} - 32\bar{t}\bar{t}^5\bar{t}^5H_{0,0,-1}(t)P_{27} \right. \right. \\
 & \left. \left. - 4\bar{t}\bar{t}^5\bar{t}^5H_{0,\{3,0\},0}(t)P_{28} + 8\bar{t}\bar{t}^5\bar{t}^5H_{0,\{3,0\},-1}(t)P_{28} - 8\bar{t}\bar{t}^5\bar{t}^5H_{0,\{3,1\},0}(t)P_{28} \right. \right.
 \end{aligned}$$

$$\begin{aligned}
& +16\hat{t}\hat{t}^5\hat{t}^5 H_{0,\{3,1\},-1}(t)P_{28}-4\hat{t}\hat{t}^5\hat{t}^5\zeta_3 P_{29}-8\hat{t}\hat{t}^5\hat{t}^5 H_{0,-1,0}(t)P_{30} \\
& +16\hat{t}\hat{t}^5\hat{t}^5 H_{0,-1,-1}(t)P_{30}+8\hat{t}\hat{t}^5\hat{t}^5 H_{0,0,0}(t)P_{31}+2\hat{t}\hat{t}^4\hat{t}^4\hat{t}^2 H_{0,0}(t)P_{34} \\
& -2\hat{t}\hat{t}^4\hat{t}^4\hat{t}^2 H_{0,-1}(t)P_{36}-2\hat{t}\hat{t}^4\hat{t}^4\hat{t}^2 H_{-1,0}(t)P_{36}+4\hat{t}\hat{t}^4\hat{t}^4\hat{t}^2 H_{-1,-1}(t)P_{36} \\
& -3t(1+4t+t^2)\bar{t}^4\hat{t}^4 P_{24}+i\pi\left(16t^2\hat{t}\hat{t}^5\hat{t}^5 H_{0,0}(t)P_{26}-2\hat{t}\hat{t}^4\hat{t}^4\hat{t}^2 H_0(t)P_{33}\right. \\
& -3t(1+4t+t^2)\bar{t}^3\hat{t}^3\hat{t}P_{24}-24\hat{t}\hat{t}H_{\{3,0\},0}(t)-48\hat{t}\hat{t}H_{\{3,1\},0}(t)+64\hat{t}\hat{t}H_{\{4,1\},0}(t) \\
& +16t(1+4t+t^2)\hat{t}\hat{t}^2 H_{-1,0}(t)+16t^2\hat{t}\hat{t}^2\zeta_2\left.)+3t(-1+2t)(1+4t+t^2)\bar{t}^4\hat{t}^3\hat{t}P_{24}H_0(t)\right. \\
& -3t(1+4t+t^2)\bar{t}^4\hat{t}^2\hat{t}P_{24}H_{-1}(t)-16\hat{t}\hat{t}H_{0,0,1}(z)-8\hat{t}\hat{t}H_{0,1,0}(z)-24\hat{t}\hat{t}H_{1,0,0}(z) \\
& -16\hat{t}\hat{t}H_{1,0,1}(z)-8\hat{t}\hat{t}H_{1,1,0}(z)-36\hat{t}\hat{t}H_{\{3,0\},0,0}(t)-72\hat{t}\hat{t}H_{\{3,1\},0,0}(t) \\
& +112\hat{t}\hat{t}H_{\{4,1\},0,0}(t)-32\hat{t}\hat{t}H_{\{4,1\},0,-1}(t)-16\hat{t}\hat{t}H_{\{4,1\},\{3,0\},0}(t)+32\hat{t}\hat{t}H_{\{4,1\},\{3,0\},-1}(t) \\
& -32\hat{t}\hat{t}H_{\{4,1\},\{3,1\},0}(t)+64\hat{t}\hat{t}H_{\{4,1\},\{3,1\},-1}(t)+24t(3+8t+3t^2)\hat{t}\hat{t}^2 H_{-1,0,0}(t) \\
& -96\hat{t}\hat{t}H_{-1,0,-1}(t)-96\hat{t}\hat{t}H_{-1,-1,0}(t)+192\hat{t}\hat{t}H_{-1,-1,-1}(t)+\left(-4\hat{t}\hat{t}^5\hat{t}^5 H_0(t)P_{32}\right. \\
& \left.+4\hat{t}\hat{t}^4\hat{t}^4\hat{t}^2 P_{35}-40\hat{t}\hat{t}H_1(z)-112\hat{t}\hat{t}H_{\{4,1\}}(t)+16t(3+2t+3t^2)\hat{t}\hat{t}^2 H_{-1}(t)\right)\zeta_2\left.\right\} \\
& +\delta_{ud,W}.
\end{aligned} \tag{4.44}$$

The polynomials here are defined as

$$\begin{aligned}
P_{16} &= 19t^4 - 56t^3 + 86t^2 - 56t + 19. \\
P_{17} &= 2t^6 - 2t^5 + t^4 + 4t^3 + t^2 - 2t + 2. \\
P_{18} &= 3t^6 - 2t^5 + 3t^4 + 4t^3 + 3t^2 - 2t + 3. \\
P_{19} &= 11t^6 - 8t^5 + 10t^4 + 16t^3 + 10t^2 - 8t + 11. \\
P_{20} &= t^8 + 2t^6 + 6t^4 + 2t^2 + 1. \\
P_{21} &= 3t^8 - 4t^7 + 10t^6 - 4t^5 + 12t^4 + 4t^3 - 2t^2 + 4t + 1. \\
P_{22} &= 9t^8 - 16t^7 + 34t^6 - 16t^5 + 30t^4 + 16t^3 - 14t^2 + 16t + 1. \\
P_{23} &= 13t^8 - 12t^7 + 38t^6 - 12t^5 + 60t^4 + 12t^3 + 2t^2 + 12t + 7. \\
P_{24} &= t^4 - t^3 - 2t^2 - t + 1. \\
P_{25} &= t^4 + 2t^3 + 5t^2 + 2t + 1. \\
P_{26} &= 2t^9 + t^8 - 12t^7 - 2t^6 + 26t^5 - 6t^3 + 2t^2 + 2t - 1. \\
P_{27} &= 3t^{10} - 15t^8 + 30t^6 - 10t^4 + 5t^2 - 1. \\
P_{28} &= 5t^{10} - 25t^8 + 50t^6 + 10t^4 - 5t^2 + 1. \\
P_{29} &= 5t^{10} + 4t^9 - 33t^8 - 8t^7 + 74t^6 + 6t^4 + 8t^3 - 7t^2 - 4t + 3. \\
P_{30} &= 7t^{10} - 35t^8 + 70t^6 - 50t^4 + 25t^2 - 5. \\
P_{31} &= 12t^{10} + 3t^9 - 66t^8 - 6t^7 + 138t^6 - 38t^4 + 6t^3 + 16t^2 - 3t - 2. \\
P_{32} &= 13t^{10} + 8t^9 - 81t^8 - 16t^7 + 178t^6 - 78t^4 + 16t^3 + 31t^2 - 8t - 3. \\
P_{33} &= t^{12} - 2t^{11} + 6t^{10} + 24t^9 - 5t^8 - 134t^7 - 212t^6 - 134t^5 - 5t^4 + 24t^3 \\
& \quad + 6t^2 - 2t + 1.
\end{aligned}$$

$$\begin{aligned}
P_{34} &= t^{12} + 2t^{11} - 10t^{10} - 56t^9 + 26t^8 + 222t^7 + 386t^6 + 222t^5 + 26t^4 - 56t^3 \\
&\quad - 10t^2 + 2t + 1. \\
P_{35} &= 2t^{12} - 2t^{11} + 8t^{10} + 16t^9 - 3t^8 - 138t^7 - 198t^6 - 138t^5 - 3t^4 + 16t^3 \\
&\quad + 8t^2 - 2t + 2. \\
P_{36} &= 5t^{12} - 2t^{11} - 2t^{10} - 40t^9 + 37t^8 + 42t^7 + 136t^6 + 42t^5 + 37t^4 - 40t^3 \\
&\quad - 2t^2 - 2t + 5.
\end{aligned}$$

$\delta_{u\bar{d},W}$ also stems solely from the non-abelian WWZ vertex and is given by

$$\begin{aligned}
\delta_{u\bar{d},W} &= (c_u - c_d)^2 C_F \left\{ -6 - \frac{13z}{2} + i\pi \left(-\frac{1}{2}(1-t)\tilde{t}(3+4z)\bar{z} - \bar{z}H_0(t) - 4z(2+z)\bar{z}H_{0,0}(t) \right. \right. \\
&\quad \left. \left. + 8z(2+z)\bar{z}H_{-1,0}(t) + 4z(2+z)\bar{z}\zeta_2 \right) + \frac{1}{2}(-1+2t)\tilde{t}(3+4z)\bar{z}H_0(t) \right. \\
&\quad - \frac{1}{2}(1+z)(4+5z)\bar{z}H_0(z) - \frac{1}{2}(3+4z)\bar{z}H_{-1}(t) - \bar{z}H_{0,0}(t) - \bar{z}H_{0,-1}(t) - \bar{z}H_{-1,0}(t) \\
&\quad \left. + 2\bar{z}H_{-1,-1}(t) - 6z(2+z)\bar{z}H_{0,0,0}(t) + 12z(2+z)\bar{z}H_{-1,0,0}(t) \right. \\
&\quad \left. + \left(2\bar{z} + 8z(2+z)\bar{z}H_0(t) - 16z(2+z)\bar{z}H_{-1}(t) \right) \zeta_2 + 4z(2+z)\bar{z}\zeta_3 \right\}. \tag{4.45}
\end{aligned}$$

4.6 Checks

In the soft-collinear (threshold) limit, the photonic part ($\Delta_\gamma^{(1,1)}$) behaves like NNLO QCD, as the massless photon can be soft and mimic the threshold behavior of massless gluon. Hence, we find presence of up to third order (\mathcal{D}_3) threshold logarithmic contributions. On the other hand, since the Z and W are massive, they do not contribute to the threshold behavior; this fact is also reflected by the presence of only \mathcal{D}_1 in their contribution, similar to the NLO QCD case.

As mentioned earlier, we have cross-checked our results at several stages of our calculation. The form factors have been checked with [31, 88, 98]. We have found complete agreement analytically to [31] by comparing the mixed NNLO QCD \times QED results. In ref. [37] the on-shell Z production and its subsequent decay have been studied at fully differential level, and the total cross-section have been extracted via a Monte Carlo integrator. We have had the possibility to perform detailed checks of these two completely independent methodologies in the evaluation of the total cross section. We have found very good agreement and perfectly compatible results, within the uncertainty bands of the numerical results of ref. [37], when comparing our predictions based on a fully analytical expression with those based on the numerical integration of the real-virtual and double-real contributions. The different gauge choices have been checked to be exactly equivalent. The mass expansion adopted in the present paper turns out to be accurate.

5 Phenomenology

In this section we present the numerical results for the inclusive total cross section for the production of an on-shell Z boson in proton-antiproton collisions at the Tevatron,

with a collider center-of-mass energy $\sqrt{S} = 1.96$ TeV, and in proton-proton collisions at the LHC, with different energies ($\sqrt{S} = 7, 8, 13, 14, 100$ TeV). They are computed using the following values of the input parameters: $m_H = 125.0$ GeV, $m_W = 80.358$ GeV, $m_Z = 91.1535$ GeV, $m_t = 173.2$ GeV, $\alpha^{-1} = 137.035999074$, $G_\mu = 1.1663781 \cdot 10^{-5}$ GeV⁻² and $\Delta\alpha_{\text{had}}(m_Z) = 0.027572$, where m_t and m_H are the top quark and Higgs boson masses.⁵ We consider 5 active flavours in the proton. In the $b\bar{b}$ channel, at NLO-EW, we include the exact dependence on m_t . At NNLO QCD-EW, we instead use the same amplitudes computed for a generic massless quark doublet, for the $d\bar{d}$ -initiated channel. We consider this approximation acceptable from a phenomenological point of view, based on the estimate done at NLO-EW for the size of the m_t effect, compared to the massless limit. We choose different parametrisations of the proton structure and for each set of parton density functions (PDFs) we consider two variants: one determination uses only QCD matrix elements and DGLAP QCD evolution, while the other relies on the same data set but adopts QCD+EW matrix elements and DGLAP QCD+QED evolution. We considered three pairs of PDF sets: NNPDF31_nnlo_as_0118 and NNPDF31_nnlo_as_0118_luxqed [101], MMHT2015_nnlo and MMHT2015qed_nnlo [102], and CT18NNLO [103] and CT18qed [104]. We have used the packages GiNaC [79, 105], handyG [106] and HarmonicSums [107–109], for manipulation and numerical evaluation of all the polylogarithmic functions which appear in the final expressions of our results.

To present the results, we consider three different approximations of the total cross section: one that includes only QCD radiative corrections $\sigma_{\text{QCD}} \equiv \sigma^{(0,0)} + \alpha_s \sigma^{(1,0)} + \alpha_s^2 \sigma^{(2,0)}$, a second one where we add to the QCD prediction the NLO-EW effects $\sigma_{\text{QCD+EW,add}} \equiv \sigma_{\text{QCD}} + \alpha \sigma^{(0,1)}$, and eventually the one that represents our complete prediction with EW and mixed QCD-EW corrections $\sigma_{\text{QCD}\times\text{EW}} \equiv \sigma^{(0,0)} + \alpha_s \sigma^{(1,0)} + \alpha \sigma^{(0,1)} + \alpha \alpha_s \sigma^{(1,1)} + \alpha_s^2 \sigma^{(2,0)}$ where $\sigma^{(i,j)}$ indicates the sole contribution from the relative perturbative order $\mathcal{O}(\alpha_s^i \alpha^j)$ with respect to the Born. In the σ_{QCD} prediction the PDFs encode the effect of the EW corrections in their parameterisation, while their perturbative evolution is driven only by the QCD kernel. On the other hand, in $\sigma_{\text{QCD}\times\text{EW}}$ the PDFs should be extracted including NLO-EW corrections in the matrix elements used to fit the data⁶ and are evolved with QCD+QED DGLAP kernels. The main component available in all the considered sets is the photon density, which fulfils the constraints imposed by the so called LUX-qed model. In the latter, the photon density is connected by an exact relation to the hadronic tensor and the proton structure functions [110].

The two models, the one with only QCD radiative corrections and the one with a complete QCD and EW analysis, consistently yield a possible description of the proton-proton scattering. For this reason, we then consider the two predictions σ_{QCD} and $\sigma_{\text{QCD}\times\text{EW}}$ as possible alternatives for the best predictions of the on-shell Z production cross section, a classical benchmark used to compare different proton parameterisations. The $\sigma_{\text{QCD}\times\text{EW}}$ is preferred, for its richer perturbative content. The difference between the two cross sections can thus be taken as an estimate of the impact of the NLO-EW and of the NNLO mixed

⁵The m_W and m_Z values are chosen considering a constant decay width definition in the gauge boson propagators and are consistent with those reported in the PDG [100], determined with a running width.

⁶A complete systematic analysis including all the NLO-EW corrections is in progress.

collider	PDF set	σ_{QCD}	$\sigma_{\text{QCD}\times\text{EW}}$	$\delta_{\text{QCD}\times\text{EW}}$	Δ_{env}	δ_{PDF}
$p\bar{p}$ 1.96 TeV	NNPDF3.1	7710.0	7649.5	-0.8	0.3%	+1.7% -1.7%
	CT18	7683.8	7640.7	-0.6		+1.6% -2.3%
	MMHT2015	7701.1	7625.8	-1.0		+2.4% -2.4%
LHC 7 TeV	NNPDF3.1	29356.2	29120.4	-0.8	1.8%	+0.9% -0.9%
	CT18	28836.9	28702.4	-0.5		+1.5% -2.4%
	MMHT2015	29023.0	28709.1	-1.1		+2.0% -2.1%
LHC 8 TeV	NNPDF3.1	34116.0	33840.2	-0.8	1.6%	+0.8% -0.8%
	CT18	33562.2	33407.5	-0.5		+1.6% -2.4%
	MMHT2015	33792.4	33420.8	-1.1		+2.0% -2.1%
LHC 13 TeV	NNPDF3.1	57769.1	57287.6	-0.8	1.1%	+0.8% -0.8%
	CT18	57152.1	56898.9	-0.4		+1.9% -2.5%
	MMHT2015	57564.8	56899.3	-1.2		+2.1% -2.1%
LHC 14 TeV	NNPDF3.1	62454.4	61931.2	-0.8	1.0%	+0.8% -0.8%
	CT18	61840.8	61568.1	-0.4		+2.0% -2.5%
	MMHT2015	62278.6	61553.7	-1.2		+2.2% -2.2%
LHC 100 TeV	NNPDF3.1	418617	412815	-1.4	2.4%	+3.1% -3.1%
	CT18	420218	418344	-0.4		+5.5% -3.8%
	MMHT2015	410367	405238	-1.2		+6.4% -4.4%

Table 1. Cross sections for on-shell Z production, expressed in picobarns and computed with different PDF sets at different collider types and energies. The two columns show the results obtained with PDF parameterisations determined with a QCD-only analysis or including also EW effects. We define $\delta_{\text{QCD}\times\text{EW}} = 100 (\sigma_{\text{QCD}\times\text{EW}}/\sigma_{\text{QCD}} - 1)$, while Δ_{env} is the percentage width of the envelope of the three PDF sets predictions in the QCD model, with respect to their mean value. The experimental PDF uncertainty δ_{PDF} in the QCD model is computed according to the definitions of each group.

QCD-EW corrections on this observable.⁷ We observe in table 1 that different PDF choices lead to a spread in the central value prediction; comparing the width of their envelope with the mean value of the three predictions, in the QCD-only case, we observe a dispersion of the results Δ_{env} ranging between the $\mathcal{O}(1\%)$ and the $\mathcal{O}(2\%)$ level at the LHC energies, while a smaller value is observed at the Tevatron. This spread is compatible with the estimate of the PDF uncertainty evaluated according to the Monte Carlo or Hessian recipes used by each PDF collaboration. We remark that the PDF uncertainties range between the $\mathcal{O}(1\%)$

⁷The inclusion in the future of N3LO results with the (today still missing) appropriate N3LO PDFs might partially interfere with our discussion, inducing a different mixture of the various partonic channels.

and the $\mathcal{O}(\pm 2.5\%)$ level, depending on the energy, collider and PDF fitting group; larger values are instead obtained for a collider with $\sqrt{S} = 100$ TeV.

For each PDF set, the shift induced by the inclusion of the NLO-EW and NNLO QCD-EW corrections is almost independent of collider and energy and ranges between -0.4% and -1.4% . The size of this shift of the central value is significant if compared with the residual subpercent QCD scale uncertainty reported in refs. [12, 13] at N³LO QCD, but also with the corresponding estimate made at NNLO-QCD.

Since the parameterisation of the proton must fulfil the sum rules expressing charge and momentum conservation, then the presence of the photon density in the proton implies a reduction of the total momentum fraction carried by quarks and gluons. In turn, we observe a reduction of the cross section of the partonic channels induced by quarks and gluons, which in general should be compensated by the positive cross section of the additional photon-induced channels. We remark that a similar $\mathcal{O}(1\%)$ reduction of the quark- and gluon-induced DY cross section for the production of a lepton pair is balanced by the contribution of the $\gamma\gamma \rightarrow \ell^+\ell^-$ process, of comparable size [25, 27, 111]. In the specific case of on-shell Z production, the $\gamma\gamma$ initial state does not contribute at $\mathcal{O}(\alpha\alpha_s)$, but only at $\mathcal{O}(\alpha^2)$; its absence explains, at technical level, the size and sign of the observed effects.

The relevance of the total on-shell Z production cross section as a standard candle for benchmarking purposes is well established. In the present study, it allows to observe how different PDF collaborations have implemented the QCDxQED evolution and the photon-density, with a different impact with respect to the corresponding pure QCD analysis.

The high-precision determination of the input parameters of the SM lagrangian is performed at hadron colliders with a template fit approach. The experimental kinematical distributions are compared with the corresponding theoretical predictions, keeping the lagrangian inputs as fitting parameters. The theoretical uncertainties contribute to the theoretical systematic error on the result of the fits [112, 113]. In this perspective, the inclusion of higher-order corrections, like the ones presented in this paper, reduces the perturbative uncertainty, leaving the PDF uncertainty as one of the main sources in the final error budget.

An important remark is related to the correlation between the SM parameter under study and the proton parameterisation in terms of replicas; a well known example is offered by the effective weak mixing angle determination from the study in the NC DY process of the invariant mass distribution of the forward-backward asymmetry. The region outside the Z resonance is weakly sensitive to the weak mixing angle but can help profiling the PDF replicas. In this spirit, the availability of higher-order radiative corrections to all the possible partonic channels contributing to a given final state puts severe constraints on their mutual interplay, yielding in turn a more effective profiling action. The corrections presented in this paper are part of the complete set necessary to describe at $\mathcal{O}(\alpha\alpha_s)$ the NC DY process, illustrated in refs. [39, 40].

In table 2 we present the width of the QCD scale uncertainty band, evaluated considering independent variations of the renormalisation scale $\mu_R = \xi_R m_Z$ and factorisation scale $\mu_F = \xi_F m_Z$. We consider 9 combinations obtained varying $\xi_{R,F} \in [\frac{1}{2}, 1, 2]$ and we discard the two cases $\xi_R = \frac{1}{2}, \xi_F = 2$ and $\xi_R = 2, \xi_F = \frac{1}{2}$. The percentage correction is computed

collider	σ_{QCD}	$\delta_{7\text{pts}}$	$\sigma_{\text{QCD+EW,add}}$	$\delta_{7\text{pts}}$	$\sigma_{\text{QCD}\times\text{EW}}$	$\delta_{7\text{pts}}$
$p\bar{p}$ 1.96 TeV	7710.0	+0.48% -0.66%	7654.0	+0.49% -0.67%	7649.5	+0.47% -0.66%
LHC 7 TeV	29356.2	+0.52% -0.26%	29135.7	+0.52% -0.24%	29120.4	+0.54% -0.27%
LHC 8 TeV	34116.0	+0.58% -0.30%	33858.7	+0.58% -0.28%	33840.2	+0.60% -0.31%
LHC 13 TeV	57769.1	+0.78% -0.45%	57325.0	+0.77% -0.42%	57287.6	+0.80% -0.45%
LHC 14 TeV	62454.4	+0.80% -0.47%	61972.6	+0.80% -0.44%	61931.2	+0.82% -0.47%
LHC 100 TeV	418617	+1.26% -1.16%	413294	+1.24% -1.12%	412815	+1.28% -1.16%

Table 2. Dependence of the cross sections for on-shell Z production, in picobarns, on the renormalisation and factorisation scale choices. The upper and lower percentage variations, compared to the central scales choice, is computed among 7 scales combinations (cfr. text). The results have been computed with the central replica of the NNPDF31_nnlo_as_0118 and NNPDF31_nnlo_as_0118_luxqed PDF sets.

collider	σ_{QCD}	δ_{QCD}	$\sigma_{\text{QCD+EW,add}}$	$\delta_{\text{QCD+EW,add}}$	$\sigma_{\text{QCD}\times\text{EW}}$	$\delta_{\text{QCD}\times\text{EW}}$
$p\bar{p}$ 1.96 TeV	7710.0	3.5	7654.0	1.1	7649.5	0.3
LHC 7 TeV	29356.2	3.5	29135.6	0.9	29120.4	0.2
LHC 8 TeV	34116.0	3.5	33858.7	0.9	33840.2	0.2
LHC 13 TeV	57769.1	3.5	57324.9	0.8	57287.7	0.2
LHC 14 TeV	62454.4	3.5	61972.6	0.8	61931.2	0.2
LHC 100 TeV	418616	3.5	413294	0.7	412815	0.1

Table 3. Cross sections computed in the G_μ and $\alpha(0)$ input schemes and expressed in picobarn. The percentage spread $\delta \equiv 100 (\sigma^{G_\mu} / \sigma^{\alpha(0)} - 1)$ between the two schemes is presented next to each perturbative approximation.

with respect to the central scales choice $\xi_R = \xi_F = 1$. In the table we compare the three approximations σ_{QCD} , $\sigma_{\text{QCD+EW,add}}$, $\sigma_{\text{QCD}\times\text{EW}}$. We observe that the percentage uncertainty is almost constant, with variations at the 0.01% level, and we understand this feature because in the G_μ input scheme the size of the EW corrections is tiny, and so are the related uncertainties.

A source of theoretical uncertainty is given by the choice of the experimental values used to express the renormalised lagrangian parameters. The comparison between the G_μ and $\alpha(0)$ schemes provides a conservative assessment of the size of the missing higher-order corrections. In table 3 we illustrate the impact of the mixed QCD-EW corrections in the reduction of the spread between the predictions computed in the two input schemes. We observe that the results including only QCD corrections are only LO from the EW point of view and suffer of a large, 3.5%, input-scheme uncertainty. The inclusion of the NLO-EW corrections stabilises down to the $\mathcal{O}(1\%)$ level the uncertainty stemming from the LO term, but not the one due to the NLO-QCD corrections. The latter is compensated by the mixed NNLO QCD-EW corrections, bringing the residual discrepancy at the $\mathcal{O}(0.2\%)$ level.

6 Conclusions

We have presented the analytical expression of the total cross section for the production of an on-shell Z boson at hadron colliders. The result has been expressed in terms of generalised polylogarithmic functions. The three elliptic functions which appear in the double-real contributions have been represented via a series expansion.

These corrections stabilise the prediction of this standard candle process, by reducing the size of the uncertainty due to missing higher orders [36]. The introduction of EW and mixed QCD-EW radiative corrections requires the consistent usage of proton PDFs determined in the same theoretical framework. The comparison with the best prediction obtained in a pure QCD-based model shows that QCD-EW effects up to $\mathcal{O}(-1\%)$ have to be taken into account and are relevant for the precision determination of this cross section.

Acknowledgments

We would like to thank F. Caola, M. Delto, P.K. Dhani, M. Jaquier, J.-N. Lang, K. Melnikov, V. Ravindran and R. Rötsch for useful discussions. N.R. and A.V. are supported by the Italian Ministero della Università e della Ricerca (grant PRIN201719AVICI_01) and by the European Research Council under the European Unions Horizon 2020 research and innovation Programme (grant agreement number 740006). R.B. is partly supported by the Italian Ministero della Università e della Ricerca (MIUR) under grant PRIN 20172LNEEZ. The research of F.B. was partially supported by the ERC Starting Grant 804394 HIPQCD. R.B. and N.R. acknowledge the COST (European Cooperation in Science and Technology) Action CA16201 PARTICLEFACE for partial support.

Open Access. This article is distributed under the terms of the Creative Commons Attribution License ([CC-BY 4.0](https://creativecommons.org/licenses/by/4.0/)), which permits any use, distribution and reproduction in any medium, provided the original author(s) and source are credited.

References

- [1] CDF and D0 collaborations, *Tevatron Run II combination of the effective leptonic electroweak mixing angle*, *Phys. Rev. D* **97** (2018) 112007 [[arXiv:1801.06283](https://arxiv.org/abs/1801.06283)] [[INSPIRE](#)].
- [2] ATLAS collaboration, *Measurement of the effective leptonic weak mixing angle using electron and muon pairs from Z-boson decay in the ATLAS experiment at $\sqrt{s} = 8$ TeV*, *ATLAS-CONF-2018-037* (2018).
- [3] CDF and D0 collaborations, *2012 Update of the Combination of CDF and D0 Results for the Mass of the W Boson*, [arXiv:1204.0042](https://arxiv.org/abs/1204.0042) [[INSPIRE](#)].
- [4] ATLAS collaboration, *Measurement of the W-boson mass in pp collisions at $\sqrt{s} = 7$ TeV with the ATLAS detector*, *Eur. Phys. J. C* **78** (2018) 110 [*Erratum ibid.* **78** (2018) 898] [[arXiv:1701.07240](https://arxiv.org/abs/1701.07240)] [[INSPIRE](#)].
- [5] G. Altarelli, R.K. Ellis and G. Martinelli, *Large Perturbative Corrections to the Drell-Yan Process in QCD*, *Nucl. Phys. B* **157** (1979) 461 [[INSPIRE](#)].

- [6] R. Hamberg, W.L. van Neerven and T. Matsuura, *A complete calculation of the order α_s^2 correction to the Drell-Yan K factor*, *Nucl. Phys. B* **359** (1991) 343 [Erratum *ibid.* **644** (2002) 403] [INSPIRE].
- [7] S. Catani, L. Cieri, G. Ferrera, D. de Florian and M. Grazzini, *Vector boson production at hadron colliders: a fully exclusive QCD calculation at NNLO*, *Phys. Rev. Lett.* **103** (2009) 082001 [arXiv:0903.2120] [INSPIRE].
- [8] K. Melnikov and F. Petriello, *Electroweak gauge boson production at hadron colliders through $O(\alpha_s^2)$* , *Phys. Rev. D* **74** (2006) 114017 [hep-ph/0609070] [INSPIRE].
- [9] R.V. Harlander and W.B. Kilgore, *Next-to-next-to-leading order Higgs production at hadron colliders*, *Phys. Rev. Lett.* **88** (2002) 201801 [hep-ph/0201206] [INSPIRE].
- [10] T. Ahmed, M. Mahakhud, N. Rana and V. Ravindran, *Drell-Yan Production at Threshold to Third Order in QCD*, *Phys. Rev. Lett.* **113** (2014) 112002 [arXiv:1404.0366] [INSPIRE].
- [11] Y. Li, A. von Manteuffel, R.M. Schabinger and H.X. Zhu, *N^3 LO Higgs boson and Drell-Yan production at threshold: The one-loop two-emission contribution*, *Phys. Rev. D* **90** (2014) 053006 [arXiv:1404.5839] [INSPIRE].
- [12] C. Duhr, F. Dulat and B. Mistlberger, *Drell-Yan Cross Section to Third Order in the Strong Coupling Constant*, *Phys. Rev. Lett.* **125** (2020) 172001 [arXiv:2001.07717] [INSPIRE].
- [13] C. Duhr, F. Dulat and B. Mistlberger, *Charged current Drell-Yan production at N^3 LO*, *JHEP* **11** (2020) 143 [arXiv:2007.13313] [INSPIRE].
- [14] C. Duhr and B. Mistlberger, *Lepton-pair production at hadron colliders at N^3 LO in QCD*, arXiv:2111.10379 [INSPIRE].
- [15] G.F. Sterman, *Summation of Large Corrections to Short Distance Hadronic Cross-Sections*, *Nucl. Phys. B* **281** (1987) 310 [INSPIRE].
- [16] S. Catani and L. Trentadue, *Resummation of the QCD Perturbative Series for Hard Processes*, *Nucl. Phys. B* **327** (1989) 323 [INSPIRE].
- [17] S. Catani and L. Trentadue, *Comment on QCD exponentiation at large x* , *Nucl. Phys. B* **353** (1991) 183 [INSPIRE].
- [18] S. Moch and A. Vogt, *Higher-order soft corrections to lepton pair and Higgs boson production*, *Phys. Lett. B* **631** (2005) 48 [hep-ph/0508265] [INSPIRE].
- [19] V. Ravindran, *Higher-order threshold effects to inclusive processes in QCD*, *Nucl. Phys. B* **752** (2006) 173 [hep-ph/0603041] [INSPIRE].
- [20] S. Catani, L. Cieri, D. de Florian, G. Ferrera and M. Grazzini, *Threshold resummation at N^3 LL accuracy and soft-virtual cross sections at N^3 LO*, *Nucl. Phys. B* **888** (2014) 75 [arXiv:1405.4827] [INSPIRE].
- [21] A.H. Ajjath, G. Das, M.C. Kumar, P. Mukherjee, V. Ravindran and K. Samanta, *Resummed Drell-Yan cross-section at N^3 LL*, *JHEP* **10** (2020) 153 [arXiv:2001.11377] [INSPIRE].
- [22] S. Camarda, L. Cieri and G. Ferrera, *Drell-Yan lepton-pair production: qT resummation at N^3 LL accuracy and fiducial cross sections at N^3 LO*, *Phys. Rev. D* **104** (2021) L111503 [arXiv:2103.04974] [INSPIRE].
- [23] S. Alioli et al., *Precision studies of observables in $pp \rightarrow W \rightarrow l\nu_l$ and $pp \rightarrow \gamma, Z \rightarrow l^+l^-$ processes at the LHC*, *Eur. Phys. J. C* **77** (2017) 280 [arXiv:1606.02330] [INSPIRE].
- [24] U. Baur, O. Brein, W. Hollik, C. Schappacher and D. Wackerroth, *Electroweak radiative corrections to neutral current Drell-Yan processes at hadron colliders*, *Phys. Rev. D* **65** (2002) 033007 [hep-ph/0108274] [INSPIRE].

- [25] C.M. Carloni Calame, G. Montagna, O. Nicrosini and A. Vicini, *Precision electroweak calculation of the production of a high transverse-momentum lepton pair at hadron colliders*, *JHEP* **10** (2007) 109 [[arXiv:0710.1722](#)] [[INSPIRE](#)].
- [26] A. Arbuzov et al., *One-loop corrections to the Drell-Yan process in SANC. (II). The Neutral current case*, *Eur. Phys. J. C* **54** (2008) 451 [[arXiv:0711.0625](#)] [[INSPIRE](#)].
- [27] S. Dittmaier and M. Huber, *Radiative corrections to the neutral-current Drell-Yan process in the Standard Model and its minimal supersymmetric extension*, *JHEP* **01** (2010) 060 [[arXiv:0911.2329](#)] [[INSPIRE](#)].
- [28] L. Buonocore, M. Grazzini and F. Tramontano, *The q_T subtraction method: electroweak corrections and power suppressed contributions*, *Eur. Phys. J. C* **80** (2020) 254 [[arXiv:1911.10166](#)] [[INSPIRE](#)].
- [29] S. Dittmaier, A. Huss and C. Schwinn, *Mixed QCD-electroweak $\mathcal{O}(\alpha_s\alpha)$ corrections to Drell-Yan processes in the resonance region: pole approximation and non-factorizable corrections*, *Nucl. Phys. B* **885** (2014) 318 [[arXiv:1403.3216](#)] [[INSPIRE](#)].
- [30] S. Dittmaier, A. Huss and C. Schwinn, *Dominant mixed QCD-electroweak $\mathcal{O}(\alpha_s\alpha)$ corrections to Drell-Yan processes in the resonance region*, *Nucl. Phys. B* **904** (2016) 216 [[arXiv:1511.08016](#)] [[INSPIRE](#)].
- [31] D. de Florian, M. Der and I. Fabre, *QCD \oplus QED NNLO corrections to Drell-Yan production*, *Phys. Rev. D* **98** (2018) 094008 [[arXiv:1805.12214](#)] [[INSPIRE](#)].
- [32] L. Cieri, G. Ferrera and G.F.R. Sborlini, *Combining QED and QCD transverse-momentum resummation for Z boson production at hadron colliders*, *JHEP* **08** (2018) 165 [[arXiv:1805.11948](#)] [[INSPIRE](#)].
- [33] M. Delto, M. Jaquier, K. Melnikov and R. Röntsch, *Mixed QCD \otimes QED corrections to on-shell Z boson production at the LHC*, *JHEP* **01** (2020) 043 [[arXiv:1909.08428](#)] [[INSPIRE](#)].
- [34] R. Bonciani, F. Buccioni, R. Mondini and A. Vicini, *Double-real corrections at $\mathcal{O}(\alpha\alpha_s)$ to single gauge boson production*, *Eur. Phys. J. C* **77** (2017) 187 [[arXiv:1611.00645](#)] [[INSPIRE](#)].
- [35] R. Bonciani, F. Buccioni, N. Rana, I. Triscari and A. Vicini, *NNLO QCD \times EW corrections to Z production in the $q\bar{q}$ channel*, *Phys. Rev. D* **101** (2020) 031301 [[arXiv:1911.06200](#)] [[INSPIRE](#)].
- [36] R. Bonciani, F. Buccioni, N. Rana and A. Vicini, *Next-to-Next-to-Leading Order Mixed QCD-Electroweak Corrections to on-Shell Z Production*, *Phys. Rev. Lett.* **125** (2020) 232004 [[arXiv:2007.06518](#)] [[INSPIRE](#)].
- [37] F. Buccioni, F. Caola, M. Delto, M. Jaquier, K. Melnikov and R. Röntsch, *Mixed QCD-electroweak corrections to on-shell Z production at the LHC*, *Phys. Lett. B* **811** (2020) 135969 [[arXiv:2005.10221](#)] [[INSPIRE](#)].
- [38] L. Cieri, D. de Florian, M. Der and J. Mazzitelli, *Mixed QCD \otimes QED corrections to exclusive Drell-Yan production using the q_T -subtraction method*, *JHEP* **09** (2020) 155 [[arXiv:2005.01315](#)] [[INSPIRE](#)].
- [39] R. Bonciani et al., *Mixed Strong-Electroweak Corrections to the Drell-Yan Process*, *Phys. Rev. Lett.* **128** (2022) 012002 [[arXiv:2106.11953](#)] [[INSPIRE](#)].
- [40] T. Armadillo, R. Bonciani, S. Devoto, N. Rana and A. Vicini, *Two-loop mixed QCD-EW corrections to neutral current Drell-Yan*, [arXiv:2201.01754](#) [[INSPIRE](#)].
- [41] L. Buonocore, M. Grazzini, S. Kallweit, C. Savoini and F. Tramontano, *Mixed QCD-EW corrections to $pp \rightarrow \ell\nu_\ell + X$ at the LHC*, *Phys. Rev. D* **103** (2021) 114012 [[arXiv:2102.12539](#)] [[INSPIRE](#)].

- [42] T. Kinoshita, *Mass singularities of Feynman amplitudes*, *J. Math. Phys.* **3** (1962) 650 [INSPIRE].
- [43] T.D. Lee and M. Nauenberg, *Degenerate Systems and Mass Singularities*, *Phys. Rev.* **133** (1964) B1549 [INSPIRE].
- [44] A. Denner, G. Weiglein and S. Dittmaier, *Application of the background field method to the electroweak standard model*, *Nucl. Phys. B* **440** (1995) 95 [hep-ph/9410338] [INSPIRE].
- [45] A. Sirlin, *Radiative Corrections in the $SU(2)_L \times U(1)$ Theory: A Simple Renormalization Framework*, *Phys. Rev. D* **22** (1980) 971 [INSPIRE].
- [46] B.A. Kniehl, *Two Loop Corrections to the Vacuum Polarizations in Perturbative QCD*, *Nucl. Phys. B* **347** (1990) 86 [INSPIRE].
- [47] G. Degrossi and A. Vicini, *Two loop renormalization of the electric charge in the standard model*, *Phys. Rev. D* **69** (2004) 073007 [hep-ph/0307122] [INSPIRE].
- [48] M. Chiesa, F. Piccinini and A. Vicini, *Direct determination of $\sin^2 \theta_{eff}^l$ at hadron colliders*, *Phys. Rev. D* **100** (2019) 071302 [arXiv:1906.11569] [INSPIRE].
- [49] A. Denner, *Techniques for calculation of electroweak radiative corrections at the one loop level and results for W physics at LEP-200*, *Fortsch. Phys.* **41** (1993) 307 [arXiv:0709.1075] [INSPIRE].
- [50] F. Jegerlehner, *Hadronic contributions to the photon vacuum polarization and their role in precision physics*, *J. Phys. G* **29** (2003) 101 [hep-ph/0104304] [INSPIRE].
- [51] F. Jegerlehner, *The Muon $g-2$ in Progress*, *Acta Phys. Polon. B* **49** (2018) 1157 [arXiv:1804.07409] [INSPIRE].
- [52] A. Keshavarzi, D. Nomura and T. Teubner, *Muon $g - 2$ and $\alpha(M_Z^2)$: a new data-based analysis*, *Phys. Rev. D* **97** (2018) 114025 [arXiv:1802.02995] [INSPIRE].
- [53] M. Davier, A. Hoecker, B. Malaescu and Z. Zhang, *A new evaluation of the hadronic vacuum polarisation contributions to the muon anomalous magnetic moment and to $\alpha(m_Z^2)$* , *Eur. Phys. J. C* **80** (2020) 241 [Erratum *ibid.* **80** (2020) 410] [arXiv:1908.00921] [INSPIRE].
- [54] D. de Florian, G.F.R. Sborlini and G. Rodrigo, *QED corrections to the Altarelli-Parisi splitting functions*, *Eur. Phys. J. C* **76** (2016) 282 [arXiv:1512.00612] [INSPIRE].
- [55] C. Anastasiou and K. Melnikov, *Higgs boson production at hadron colliders in NNLO QCD*, *Nucl. Phys. B* **646** (2002) 220 [hep-ph/0207004] [INSPIRE].
- [56] C. Anastasiou, S. Buehler, C. Duhr and F. Herzog, *NNLO phase space master integrals for two-to-one inclusive cross sections in dimensional regularization*, *JHEP* **11** (2012) 062 [arXiv:1208.3130] [INSPIRE].
- [57] P. Nogueira, *Automatic Feynman graph generation*, *J. Comput. Phys.* **105** (1993) 279 [INSPIRE].
- [58] T. Hahn, *Generating Feynman diagrams and amplitudes with FeynArts 3*, *Comput. Phys. Commun.* **140** (2001) 418 [hep-ph/0012260] [INSPIRE].
- [59] J.A.M. Vermaseren, *New features of FORM*, [math-ph/0010025](#) [INSPIRE].
- [60] F.V. Tkachov, *A Theorem on Analytical Calculability of Four Loop Renormalization Group Functions*, *Phys. Lett. B* **100** (1981) 65 [INSPIRE].
- [61] K.G. Chetyrkin and F.V. Tkachov, *Integration by Parts: The Algorithm to Calculate β -functions in 4 Loops*, *Nucl. Phys. B* **192** (1981) 159 [INSPIRE].

- [62] S. Laporta, *High precision calculation of multiloop Feynman integrals by difference equations*, *Int. J. Mod. Phys. A* **15** (2000) 5087 [[hep-ph/0102033](#)] [[INSPIRE](#)].
- [63] P. Maierhöfer, J. Usovitsch and P. Uwer, *Kira — A Feynman integral reduction program*, *Comput. Phys. Commun.* **230** (2018) 99 [[arXiv:1705.05610](#)] [[INSPIRE](#)].
- [64] R.N. Lee, *LiteRed 1.4: a powerful tool for reduction of multiloop integrals*, *J. Phys. Conf. Ser.* **523** (2014) 012059 [[arXiv:1310.1145](#)] [[INSPIRE](#)].
- [65] R.N. Lee, *Presenting LiteRed: a tool for the Loop InTEgrals REDuction*, [arXiv:1212.2685](#) [[INSPIRE](#)].
- [66] A. von Manteuffel and C. Studerus, *Reduze 2 — Distributed Feynman Integral Reduction*, [arXiv:1201.4330](#) [[INSPIRE](#)].
- [67] C. Studerus, *Reduze-Feynman Integral Reduction in C++*, *Comput. Phys. Commun.* **181** (2010) 1293 [[arXiv:0912.2546](#)] [[INSPIRE](#)].
- [68] A.V. Kotikov, *Differential equations method: New technique for massive Feynman diagrams calculation*, *Phys. Lett. B* **254** (1991) 158 [[INSPIRE](#)].
- [69] E. Remiddi, *Differential equations for Feynman graph amplitudes*, *Nuovo Cim. A* **110** (1997) 1435 [[hep-th/9711188](#)] [[INSPIRE](#)].
- [70] T. Gehrmann and E. Remiddi, *Differential equations for two loop four point functions*, *Nucl. Phys. B* **580** (2000) 485 [[hep-ph/9912329](#)] [[INSPIRE](#)].
- [71] M. Argeri and P. Mastrolia, *Feynman Diagrams and Differential Equations*, *Int. J. Mod. Phys. A* **22** (2007) 4375 [[arXiv:0707.4037](#)] [[INSPIRE](#)].
- [72] J.M. Henn, *Multiloop integrals in dimensional regularization made simple*, *Phys. Rev. Lett.* **110** (2013) 251601 [[arXiv:1304.1806](#)] [[INSPIRE](#)].
- [73] J.M. Henn, *Lectures on differential equations for Feynman integrals*, *J. Phys. A* **48** (2015) 153001 [[arXiv:1412.2296](#)] [[INSPIRE](#)].
- [74] J. Ablinger, A. Behring, J. Blümlein, A. De Freitas, A. von Manteuffel and C. Schneider, *Calculating Three Loop Ladder and V-Topologies for Massive Operator Matrix Elements by Computer Algebra*, *Comput. Phys. Commun.* **202** (2016) 33 [[arXiv:1509.08324](#)] [[INSPIRE](#)].
- [75] J. Ablinger, J. Blümlein, P. Marquard, N. Rana and C. Schneider, *Automated Solution of First Order Factorizable Systems of Differential Equations in One Variable*, *Nucl. Phys. B* **939** (2019) 253 [[arXiv:1810.12261](#)] [[INSPIRE](#)].
- [76] E. Remiddi and J.A.M. Vermaseren, *Harmonic polylogarithms*, *Int. J. Mod. Phys. A* **15** (2000) 725 [[hep-ph/9905237](#)] [[INSPIRE](#)].
- [77] A. Goncharov, *Polylogarithms in arithmetic and geometry*, in *Proceedings of the International Congress of Mathematicians*, Birkhäuser, Basel (1995) pp. 374–387 [[DOI](#)].
- [78] A.B. Goncharov, *Multiple polylogarithms and mixed Tate motives*, [math/0103059](#) [[INSPIRE](#)].
- [79] J. Vollinga and S. Weinzierl, *Numerical evaluation of multiple polylogarithms*, *Comput. Phys. Commun.* **167** (2005) 177 [[hep-ph/0410259](#)] [[INSPIRE](#)].
- [80] J. Ablinger, J. Blümlein and C. Schneider, *Harmonic Sums and Polylogarithms Generated by Cyclotomic Polynomials*, *J. Math. Phys.* **52** (2011) 102301 [[arXiv:1105.6063](#)] [[INSPIRE](#)].
- [81] J. Fleischer, A.V. Kotikov and O.L. Veretin, *The Differential equation method: Calculation of vertex type diagrams with one nonzero mass*, *Phys. Lett. B* **417** (1998) 163 [[hep-ph/9707492](#)] [[INSPIRE](#)].

- [82] J. Fleischer, A.V. Kotikov and O.L. Veretin, *Analytic two loop results for selfenergy type and vertex type diagrams with one nonzero mass*, *Nucl. Phys. B* **547** (1999) 343 [[hep-ph/9808242](#)] [[INSPIRE](#)].
- [83] U. Aglietti and R. Bonciani, *Master integrals with one massive propagator for the two loop electroweak form-factor*, *Nucl. Phys. B* **668** (2003) 3 [[hep-ph/0304028](#)] [[INSPIRE](#)].
- [84] U. Aglietti and R. Bonciani, *Master integrals with 2 and 3 massive propagators for the 2 loop electroweak form-factor — planar case*, *Nucl. Phys. B* **698** (2004) 277 [[hep-ph/0401193](#)] [[INSPIRE](#)].
- [85] U. Aglietti, R. Bonciani, G. Degrassi and A. Vicini, *Master integrals for the two-loop light fermion contributions to $gg \rightarrow H$ and $H \rightarrow \gamma\gamma$* , *Phys. Lett. B* **600** (2004) 57 [[hep-ph/0407162](#)] [[INSPIRE](#)].
- [86] U. Aglietti, R. Bonciani, L. Grassi and E. Remiddi, *The Two loop crossed ladder vertex diagram with two massive exchanges*, *Nucl. Phys. B* **789** (2008) 45 [[arXiv:0705.2616](#)] [[INSPIRE](#)].
- [87] R. Bonciani, G. Degrassi and A. Vicini, *On the Generalized Harmonic Polylogarithms of One Complex Variable*, *Comput. Phys. Commun.* **182** (2011) 1253 [[arXiv:1007.1891](#)] [[INSPIRE](#)].
- [88] A. Kotikov, J.H. Kühn and O. Veretin, *Two-Loop Formfactors in Theories with Mass Gap and Z-Boson Production*, *Nucl. Phys. B* **788** (2008) 47 [[hep-ph/0703013](#)] [[INSPIRE](#)].
- [89] J.M. Henn, A.V. Smirnov and V.A. Smirnov, *Evaluating Multiple Polylogarithm Values at Sixth Roots of Unity up to Weight Six*, *Nucl. Phys. B* **919** (2017) 315 [[arXiv:1512.08389](#)] [[INSPIRE](#)].
- [90] A.V. Smirnov, *FIESTA4: Optimized Feynman integral calculations with GPU support*, *Comput. Phys. Commun.* **204** (2016) 189 [[arXiv:1511.03614](#)] [[INSPIRE](#)].
- [91] J. Broedel, C. Duhr, F. Dulat, B. Penante and L. Tancredi, *Elliptic polylogarithms and Feynman parameter integrals*, *JHEP* **05** (2019) 120 [[arXiv:1902.09971](#)] [[INSPIRE](#)].
- [92] S. Pozzorini and E. Remiddi, *Precise numerical evaluation of the two loop sunrise graph master integrals in the equal mass case*, *Comput. Phys. Commun.* **175** (2006) 381 [[hep-ph/0505041](#)] [[INSPIRE](#)].
- [93] J. Blümlein and C. Schneider, *The Method of Arbitrarily Large Moments to Calculate Single Scale Processes in Quantum Field Theory*, *Phys. Lett. B* **771** (2017) 31 [[arXiv:1701.04614](#)] [[INSPIRE](#)].
- [94] R.N. Lee, A.V. Smirnov and V.A. Smirnov, *Solving differential equations for Feynman integrals by expansions near singular points*, *JHEP* **03** (2018) 008 [[arXiv:1709.07525](#)] [[INSPIRE](#)].
- [95] R.N. Lee, A.V. Smirnov and V.A. Smirnov, *Evaluating ‘elliptic’ master integrals at special kinematic values: using differential equations and their solutions via expansions near singular points*, *JHEP* **07** (2018) 102 [[arXiv:1805.00227](#)] [[INSPIRE](#)].
- [96] R. Bonciani, G. Degrassi, P.P. Giardino and R. Gröber, *A Numerical Routine for the Crossed Vertex Diagram with a Massive-Particle Loop*, *Comput. Phys. Commun.* **241** (2019) 122 [[arXiv:1812.02698](#)] [[INSPIRE](#)].
- [97] J. Blümlein, P. Marquard, N. Rana and C. Schneider, *The Heavy Fermion Contributions to the Massive Three Loop Form Factors*, *Nucl. Phys. B* **949** (2019) 114751 [[arXiv:1908.00357](#)] [[INSPIRE](#)].

- [98] A.H. Ajjath et al., *NNLO $QCD \oplus QED$ corrections to Higgs production in bottom quark annihilation*, *Phys. Rev. D* **100** (2019) 114016 [[arXiv:1906.09028](#)] [[INSPIRE](#)].
- [99] J. Ablinger et al., *Heavy quark form factors at two loops*, *Phys. Rev. D* **97** (2018) 094022 [[arXiv:1712.09889](#)] [[INSPIRE](#)].
- [100] PARTICLE DATA GROUP collaboration, *Review of Particle Physics*, *PTEP* **2020** (2020) 083C01 [[INSPIRE](#)].
- [101] NNPDF collaboration, *Parton distributions from high-precision collider data*, *Eur. Phys. J. C* **77** (2017) 663 [[arXiv:1706.00428](#)] [[INSPIRE](#)].
- [102] L.A. Harland-Lang, A.D. Martin, R. Nathvani and R.S. Thorne, *Ad Lucem: QED Parton Distribution Functions in the MMHT Framework*, *Eur. Phys. J. C* **79** (2019) 811 [[arXiv:1907.02750](#)] [[INSPIRE](#)].
- [103] T.-J. Hou et al., *New CTEQ global analysis of quantum chromodynamics with high-precision data from the LHC*, *Phys. Rev. D* **103** (2021) 014013 [[arXiv:1912.10053](#)] [[INSPIRE](#)].
- [104] CTEQ-TEA collaboration, *The photon PDF within the CT18 global analysis*, [arXiv:2106.10299](#) [[INSPIRE](#)].
- [105] C.W. Bauer, A. Frink and R. Kreckel, *Introduction to the GiNaC framework for symbolic computation within the C++ programming language*, [cs/0004015](#).
- [106] L. Naterop, A. Signer and Y. Ulrich, *handyG —Rapid numerical evaluation of generalised polylogarithms in Fortran*, *Comput. Phys. Commun.* **253** (2020) 107165 [[arXiv:1909.01656](#)] [[INSPIRE](#)].
- [107] J. Ablinger, *A Computer Algebra Toolbox for Harmonic Sums Related to Particle Physics*, Master's thesis, Linz U., 2009 [[arXiv:1011.1176](#)] [[INSPIRE](#)].
- [108] J. Ablinger, J. Blümlein and C. Schneider, *Analytic and Algorithmic Aspects of Generalized Harmonic Sums and Polylogarithms*, *J. Math. Phys.* **54** (2013) 082301 [[arXiv:1302.0378](#)] [[INSPIRE](#)].
- [109] J. Ablinger, *The package HarmonicSums: Computer Algebra and Analytic aspects of Nested Sums*, *PoS LL2014* (2014) 019 [[arXiv:1407.6180](#)] [[INSPIRE](#)].
- [110] A. Manohar, P. Nason, G.P. Salam and G. Zanderighi, *How bright is the proton? A precise determination of the photon parton distribution function*, *Phys. Rev. Lett.* **117** (2016) 242002 [[arXiv:1607.04266](#)] [[INSPIRE](#)].
- [111] L. Buonocore, P. Nason, F. Tramontano and G. Zanderighi, *Photon and leptons induced processes at the LHC*, *JHEP* **12** (2021) 073 [[arXiv:2109.10924](#)] [[INSPIRE](#)].
- [112] C.M. Carloni Calame et al., *Precision Measurement of the W-Boson Mass: Theoretical Contributions and Uncertainties*, *Phys. Rev. D* **96** (2017) 093005 [[arXiv:1612.02841](#)] [[INSPIRE](#)].
- [113] E. Bagnaschi and A. Vicini, *Parton Density Uncertainties and the Determination of Electroweak Parameters at Hadron Colliders*, *Phys. Rev. Lett.* **126** (2021) 041801 [[arXiv:1910.04726](#)] [[INSPIRE](#)].